Muscle-resident mesenchymal progenitors sense and repair peripheral nerve injury via the GDNF-BDNF axis

Kyusang Yoo[1], Young-Woo Jo[1], Takwon Yoo[1], Sang-Hyeon Hann[1], Inkuk Park[1], Yea-Eun Kim[1], Ye Lynne Kim[1], Joonwoo Rhee[1], In-Wook Song[1], Ji-Hoon Kim[1,2], Daehyun Baek[1] and Young-Yun Kong[1*]

[1] School of Biological Sciences, Seoul National University, Seoul 08826, Republic of Korea

[2] Molecular Recognition Research Center, Korea Institute of Science and Technology, Seoul 02792, Republic of Korea

[*]Correspondence and requests for materials should be addressed to Y.Y.K. (ykong@snu.ac.kr)

Author Contributions

Conceptualization, K.Y. and Y.Y.K.; Methodology, K.Y.; Software, K.Y. and T.Y.; Validation, K.Y., Y.W.J., T.Y., D.B. and Y.Y.K.; Formal analysis, K.Y., and Y.W.J.; Investigation, K.Y. and Y.W.J.; Resources, K.Y., Y.W.J., S.H.H., I.P., Y.E.K., J.R., I.W.S. and J.H.K.; Data curation, K.Y.; Writing – original draft, K.Y.; Writing – review & editing, K.Y., Y.W.J., Y.E.K., Y.L.K. and Y.Y.K.; Visualization, K.Y., and Y.W.J.; Supervision, Y.Y.K.; Project administration, Y.Y.K.; Funding acquisition, Y.Y.K..

Declaration of interests

The authors declare no competing interests.

Abstract

Fibro-adipogenic progenitors (FAPs) are muscle-resident mesenchymal progenitors that can contribute to muscle tissue homeostasis and regeneration, as well as postnatal maturation and lifelong maintenance of the neuromuscular system. Recently, traumatic injury to the peripheral nerve was shown to activate FAPs, suggesting that FAPs can respond to nerve injury. However, questions of how FAPs can sense the anatomically distant peripheral nerve injury and whether FAPs can directly contribute to nerve regeneration remained unanswered. Here, utilizing single-cell transcriptomics and mouse models, we discovered that a subset of FAPs expressing GDNF receptors *Ret* and *Gfra1* can respond to peripheral nerve injury by sensing GDNF secreted by Schwann cells. Upon GDNF sensing, this subset becomes activated and expresses *Bdnf*. FAP-specific inactivation of *Bdnf* (*Prrx1*^{Cre}; *Bdnf*$^{fl/fl}$) resulted in delayed nerve regeneration owing to defective remyelination, indicating that GDNF-sensing FAPs play an important role in the remyelination process during peripheral nerve regeneration. In aged mice, significantly reduced *Bdnf* expression in FAPs was observed upon nerve injury, suggesting the clinical relevance of FAP-derived BDNF in the age-related delays in nerve regeneration. Collectively, our study revealed the previously unidentified role of FAPs in peripheral nerve regeneration, and the molecular mechanism behind FAPs' response to peripheral nerve injury.

Introduction

Positioned in the interstitial space between myofibers (Uezumi et al., 2010), fibro-adipogenic progenitors (FAPs) interact with cellular components within skeletal muscle to ensure normal development, homeostasis, and regeneration of muscle tissue. During developmental myogenesis, embryonic FAPs expressing *Osr1* contribute to limb muscle patterning by regulating the expression of extracellular matrix (ECM) genes that make up muscle connective tissue (Vallecillo-Garcia et al., 2017). In young adults, FAPs are necessary for normal growth and long-term maintenance of skeletal muscle, which otherwise undergo progressive muscle atrophy in the absence of PDGFRα^{+} FAPs (Roberts et al., 2013; Wosczyna et al., 2019; Uezumi et al., 2021). Upon muscle injury, FAPs proliferate in response to IL-4/IL-13 signals from eosinophils, and participate in clearing of necrotic debris via phagocytosis (Heredia et al., 2013). Also, the proliferated FAPs regulate expansion and asymmetric commitment of muscle stem cells (MuSCs) via secreted factors such as WISP1, leading to robust *de novo* myofiber formation (Joe et al., 2010; Lukjanenko et al., 2019; Wosczyna et al., 2019). Conversely, absence of FAPs or its functional decline with age cause premature differentiation of MuSCs upon injury, resulting in formation of smaller regenerated myofibers (Murphy et al., 2011; Lukjanenko et al., 2019; Wosczyna et al., 2019). After sufficient regeneration of myofibers occurs, FAPs undergo apoptosis via TNF signaling from monocyte/macrophages, such that its numbers return to those of unperturbed muscles (Lemos et al., 2015; Saito et al., 2020). Failure to remove excess FAPs after muscle regeneration results in unwanted fibrosis, which compromises muscle function (Uezumi et al., 2011; Uezumi et al., 2014).

62 In addition to formation and maintenance of muscle tissue, FAPs also contribute to maturation
63 and maintenance of the neural components within skeletal muscle. Previously, we reported that
64 FAPs promote postsynaptic maturation of the neuromuscular junction (NMJ) through the
65 BAP1/SMN axis during postnatal development (Kim et al., 2022). Selective inactivation of
66 *Bap1* in FAPs results in dysfunctional NMJs, with sustained expression of the immature form
67 of acetylcholine receptor subunit, *AchRγ*, in skeletal muscle (Kim et al., 2022). Progressively,
68 these mice exhibit denervation at the NMJ, retraction of motor axons, reduction of myelination
69 and axon diameter, and eventually motor neuron loss, suggesting that FAPs prevent the dying-
70 back loss of motor neurons (Kim et al., 2022). Recently, we also reported defective presynaptic
71 maturation and maintenance in mice with selective *Smn* downregulation in FAPs, again
72 suggesting the role of FAPs in postnatal NMJ development (Hann et al., 2024). In adult mice,
73 BMP3B secretion by FAPs stabilize NMJs and Schwann cells by promoting the myelination
74 program in Schwann cells, thereby directly contributing to the maintenance of neural
75 components within skeletal muscle (Uezumi et al., 2021). In the absence of FAPs or *Bmp3b*,
76 mice exhibit muscle weakness and myofiber atrophy along with destabilization of Schwann
77 cells and denervation at NMJs, which closely resemble the phenotypes observed in age-related
78 sarcopenia (Uezumi et al., 2021). Similarly, conditional deletion of *Bap1* in FAPs in adulthood
79 cause denervation at the NMJs and eventually loss of motor neurons, demonstrating the
80 requirement of FAPs in maintaining the neuromuscular system (Kim et al., 2022). Conversely,
81 disturbance in the neural component can influence the behavior of FAPs; for instance,
82 denervation is known to activate FAPs (Contreras et al., 2016; Gonzalez et al., 2017; Madaro
83 et al., 2018). This suggests that FAPs can somehow sense the anatomically distant peripheral
84 nerve injury. However, the question of how FAPs are able to sense the distant peripheral nerve

injury remains unanswered (Theret et al., 2021). Furthermore, whether FAPs are actually able to exert beneficial effects on peripheral nerve regeneration remains elusive.

In accordance with its various functions, heterogeneity within FAPs began to be recognized with the advent of single-cell analysis technology (Contreras et al., 2021). By profiling the expression levels of 87-selected genes in isolated singlets of FAPs, dynamic transitions between heterogeneous subpopulations of FAPs, identified by different expression levels of TIE2 and VCAM1, was observed during postnatal and regenerative myogenesis (Malecova et al., 2018). The report showed that while activation of TIE2^{high} FAPs is observed in neonatal mice, activation of VCAM1^{+} FAPs is observed in injured muscles, suggesting distinct functional involvement of FAPs in the two different contexts of myogenesis (Malecova et al., 2018). Additionally, single-cell RNA-sequencing (scRNA-seq) enabled identification of heterogeneity within FAPs based on the genome-wide transcriptome data (Lieberman et al., 2021). In homeostatic adult muscle, two distinct subpopulations within FAPs have been identified, namely *Dpp4*$^{+}$ and *Cxcl14*$^{+}$ FAPs (Scott et al., 2019; Oprescu et al., 2020). Functionally, we reported that DPP4^{+} FAPs contribute to maturation and maintenance of the neuromuscular system via the BAP1/SMN axis (Kim et al., 2022). In juvenile muscle, five different subpopulations within FAPs were characterized, each having different contexts of activation and differentiation potentials (Leinroth et al., 2022). *Osr1*$^{+}$ FAPs are precursor cells that can form all other subpopulations; *Clu*$^{+}$ FAPs are most potent in mineralization; *Adam12*$^{+}$ and *Gap43*$^{+}$ FAPs are immune-responsive; and *Hsd11b1*$^{+}$ FAPs respond to nerve transection (Leinroth et al., 2022). The different activation cues and differentiation potentials in each subpopulation of FAPs suggest distinct roles those subsets can play in different contexts of

skeletal muscle biology. Indeed, dynamic transcriptomic changes in FAP subpopulations in response to muscle injury (Scott et al., 2019; De Micheli et al., 2020; Oprescu et al., 2020) or denervation (Nicoletti et al., 2020; Proietti et al., 2021; Lin et al., 2022; Nicoletti et al., 2023) have been identified in studies that implemented scRNA-seq analysis. Still, the question of how FAPs may sense the distant nerve injury and whether FAPs can beneficially contribute to nerve regeneration remain largely unknown.

In response to nerve injury, various neurotrophic factors are expressed and secreted by the surrounding cells to facilitate regeneration. One of those neurotrophic factors is GDNF, previously reported to be expressed robustly by Schwann cells upon nerve injury (Hammarberg et al., 1996; Hoke et al., 2002; Arthur-Farraj et al., 2012; Xu et al., 2013; Proietti et al., 2021). Canonical GDNF signaling pathway involves two well-known receptors of GDNF: RET and GFRα1. Binding of GDNF to GFRα1 induces complex formation with the receptor tyrosine kinase (RTK) RET, which initiate the downstream phosphorylation cascade via autophosphorylation upon dimerization (Jing et al., 1996; Treanor et al., 1996; Trupp et al., 1996). The downstream phosphorylation cascades include the Ras-MAPK pathway, the PI3K-Akt pathway, and the Src family kinase-mediated pathway, which are known to promote neuronal survival and neurite outgrowth (Encinas et al., 2001; Sariola and Saarma, 2003). Indeed, exogenous delivery of GDNF was shown to promote motor neuron survival and enhance axonal growth upon nerve injury, which resulted in improved functional recovery (Cintron-Colon et al., 2020). Though the role and function of GDNF on the regenerating neuron have been demonstrated, other possible cellular targets of GDNF that may facilitate the nerve regeneration process remain to be studied.

131

132 Here, using the scRNA-seq approach, we aimed to identify the response mechanism of FAPs
133 to nerve injury, by uncovering its nerve injury-sensing mechanism and its potentially beneficial
134 effect on nerve regeneration. To obtain a comprehensive scRNA-seq database of FAPs'
135 response to nerve injury, FAPs from both chronic, non-regenerating nerve injury (denervation)-
136 and acute, regeneration-prone nerve injury (crush)-affected muscles were collected at different
137 time points over the course of regeneration. As a result, distinct transcriptomic profiles of FAPs
138 at different time points post the two types of nerve injuries were captured in single-cell
139 resolution, from which the response mechanism of FAPs to nerve injury was identified and
140 validated using mouse models. Specifically, we found that upon peripheral nerve injury, GDNF
141 from Schwann cells can activate FAPs, which in turn express BDNF to promote remyelination
142 during nerve regeneration. Our study suggests FAPs as an important player that actively
143 participates in the nerve regeneration process, of which we believe should be considered in
144 future studies aiming for improved understanding of the peripheral nerve regeneration process.

145

146 **Results**

147 **Distinct response profiles of FAPs upon nerve crush injury versus denervation**

148 To establish a comprehensive transcriptome database of nerve injury-affected FAPs at single-
149 cell resolution, we performed scRNA-seq using FAPs isolated from sciatic nerve crush injury
150 (SNC)- or denervation (DEN)-affected muscles at different time points over the course of
151 regeneration (Figure 1—figure supplements 1A and B). Four time points (3, 7, 14, and 28 days
152 post injury, hereafter dpi) along the regeneration process were chosen for analysis to capture

153 the transcriptomes of FAPs at both early and late stages of regeneration. Selection of such time
154 points was based on a previous report that showed the reinnervation process of the tibialis
155 anterior (TA) muscle after SNC, where Wallerian degeneration was evident at 7 dpi, and
156 reinnervation was mostly completed at 28 dpi (Magill et al., 2007). Including the uninjured
157 control, scRNA-seq data from a total of nine samples (Uninjured, SNC-3dpi, SNC-7dpi, SNC-
158 14dpi, SNC-28dpi, DEN-3dpi, DEN-7dpi, DEN-14dpi, and DEN-28dpi) were obtained via the
159 10x Genomics platform (Figure 1—figure supplement 1A). Quality control and filtering of the
160 sequenced cells yielded a total of 44,597 cells for further analysis, where 4955.2±1022.8 cells
161 were captured from each sample. Prior to downstream analysis, integration (Hao et al., 2021)
162 of our scRNA-seq data with a publicly available scRNA-seq data of mononuclear cells from
163 denervated muscles at 0, 2, 5, and 15 dpi (Nicoletti et al., 2023) was carried out for data
164 validation. Expectedly, most (97.7%) of the filtered cells in our scRNA-seq data clustered with
165 the denervation-affected FAPs in the published scRNA-seq data, confirming the validity of the
166 data produced in our study (Figure 1—figure supplements 1C and D).
167

168 To look into the chronological transcriptomic changes that occur in FAPs in response to SNC
169 or DEN on a global level, we analyzed our scRNA-seq data by samples. Visualization of the
170 scRNA-seq data on uniform manifold approximation and projection (UMAP) plots showed
171 similar changes in the early stages of regeneration (3 and 7 dpi) compared to uninjured FAPs,
172 regardless of the type of injury (Figure 1A). However, as FAPs reached later stages of
173 regeneration (14 and 28 dpi), SNC-affected FAPs returned to states similar to uninjured control,
174 while DEN-affected FAPs stayed in the activated state (Figure 1A). The similarities and
175 differences observed on the UMAP plots could also be found in the differentially expressed

176 gene (DEG) analyses as well as in the hierarchical clustering analysis using those DEGs
177 (Figures 1B–E, Figure 1—figure supplements 2A–C). As a result of pairwise DEG analyses
178 comparing all nine samples, different numbers of DEGs were identified, of which correlated
179 with the similarities between samples observed on UMAP plots (Figures 1A–E, Figure 1—
180 figure supplements 2A and B). Hierarchical clustering of the nine samples using all unique
181 DEGs identified from the pairwise comparisons showed clustering of uninjured control with
182 SNC-14dpi and SNC-28dpi, suggesting FAPs' return to homeostatic state (Figure 1—figure
183 supplement 2C). On the other hand, DEN-14dpi and DEN-28dpi clustered with each other, but
184 not with uninjured control, suggesting the chronic activation of FAPs in response to DEN as
185 reported previously (Madaro et al., 2018) (Figure 1—figure supplement 2C). Samples that
186 captured the early responses of FAPs to nerve injuries (3 or 7 dpi) were clustered together by
187 dpi rather than the type of injury, suggesting similar response profiles of FAPs to both types of
188 nerve injuries (Figure 1—figure supplement 2C). Indeed, the numbers of DEGs between SNC-
189 3dpi versus DEN-3dpi and SNC-7dpi versus DEN-7dpi were among the lowest identified in
190 the pairwise analyses (Figures 1B and C, Figure 1—figure supplement 2A). Overall, the
191 number of DEGs between SNC- and DEN-affected FAPs increased significantly with dpi,
192 showing the bifurcation of FAP's response to the different types of nerve injuries in the later
193 stages of regeneration (Figures 1B–E).

194

195 In a previous study, chronic activation of the STAT3/IL-6 pathway in FAPs in response to DEN
196 was reported (Madaro et al., 2018). Indeed, *Il6* was identified as one of the genes upregulated
197 at all four time points in response to DEN compared to uninjured control in our data (Figure
198 1—figure supplements 2D and E). Although it did not pass the fold change (FC) threshold (FC

199 >= 2) in the DEG analyses, expression of *Stat3* also showed significant chronic upregulation
200 in all DEN-affected FAPs as well (Figure 1—figure supplements 2F and G). In response to
201 SNC, however, only transient upregulation of both genes was observed (Figure 1—figure
202 supplements 2D–G).

203

204 To obtain biological insights on the different responses of FAPs to SNC versus DEN in the later
205 stage of regeneration, we subjected the two lists of genes from Figure 1E (28 dpi, SNC_UP and
206 DEN_UP) to gene set overrepresentation analysis (ORA) using g:Profiler (Kolberg et al., 2023).
207 From both sets of genes, pathways related to tissue regeneration/wound healing were enriched
208 (Figures 1F and G, Figure 1—figure supplements 3A and B). In contrast, pathways related to
209 immune cell recruitment, inflammation, and ECM regulation by collagen biosynthesis were
210 enriched specifically in DEN-28dpi (Figure 1F, Figure 1—figure supplement 3A), which is
211 consistent with the previous report that showed the direct contribution of FAPs to fibrosis in
212 denervated muscles (Contreras et al., 2016; Madaro et al., 2018). Also, mild immune cell
213 infiltration into affected muscles in response to DEN was previously described (Lin et al., 2022;
214 Nicoletti et al., 2023); our results suggest the role of FAPs in chemotactic recruitment of
215 immune cells in denervated muscles. In addition, the pathway 'negative regulation of neuron
216 apoptosis' was enriched in DEN-28dpi, suggesting a prolonged attempt of FAPs to preserve
217 neurons that must be alive for reinnervation of the denervated muscle (Figure 1F, Figure 1—
218 figure supplement 3A). On the other hand, some pathways were exclusively enriched in SNC-
219 28dpi, such as negative regulation of chemotaxis and prostaglandin metabolism (Figure 1G,
220 Figure 1—figure supplement 3B). It is generally understood that after a successful tissue
221 regeneration process, resolution of immune response allow for the tissue to return to

222 homeostasis (Ortega-Gomez et al., 2013; Aurora and Olson, 2014; Julier et al., 2017); our
223 results suggest the role of FAPs in regulating immune resolution near the end of nerve
224 regeneration. Furthermore, the role of prostaglandin in peripheral nerve regeneration has
225 recently been described (Forese et al., 2020; Bakooshli et al., 2023); our ORA results suggested
226 that FAPs may also be involved in regulation of prostaglandin levels during peripheral nerve
227 regeneration.

228

229 To discover biological pathways behind the supposedly similar responses of FAPs to both SNC
230 and DEN in the early phases of regeneration, we examined DEGs from comparing SNC-3dpi,
231 SNC-7dpi, DEN-3dpi, and DEN-7dpi to uninjured controls. Many of the upregulated genes
232 identified in the DEG analyses were shared amongst the four samples (Figure 1—figure
233 supplement 3C). ORA using the shared upregulated genes revealed enrichment in pathways
234 that were also enriched in DEN-28dpi compared to SNC-28dpi, such as immune cell
235 recruitment and ECM regulation, supporting the idea that early-activated states within FAPs
236 persist for a prolonged period in response to DEN (Figures 1F and H, Figure 1—figure
237 supplements 3A and D). Collectively, analysis of our scRNA-seq data by samples revealed
238 similar response profiles of FAPs to both SNC and DEN in the early stages of regeneration,
239 which then bifurcated into chronic activation in response to DEN and return to homeostasis in
240 response to SNC, showing correlative behaviors along with the degree of nerve regeneration
241 and target muscle reinnervation.

242

243 **Nerve injury-responsive subsets within FAPs**

Although analysis of our scRNA-seq data on the population level provided general insights on how FAPs may respond to the different types of nerve injuries, the results could not provide us with sufficient clues on how FAPs can sense nerve injuries, or how they may directly contribute to nerve regeneration. Thus, we next analyzed our scRNA-seq data on the subpopulation level, hoping to distinguish subsets within FAPs that may be more relevant to the context of sensing and responding to nerve injury. To identify distinct subsets within nerve injury-affected FAPs, we applied unsupervised clustering to the merged scRNA-seq data of all nine samples following the Seurat-R workflow (Hao et al., 2021). As a result, seven clusters with unique gene expression profiles were identified from the nerve injury-affected FAPs, with marker genes specifically expressed in each cluster (Figures 2A–C, Figure 2—figure supplement 1A).

Interestingly, while clusters 4-7 showed little or no significant change in their proportions in response to nerve injury, clusters 1-3 exhibited dramatic changes upon nerve injury (Figures 2D and E). In particular, cluster 1 was mostly present in uninjured muscles or in muscles where reinnervation had occurred to at least some degree (SNC-14dpi and SNC-28dpi) (Magill et al., 2007) (Figures 2D and E). In contrast, presence of clusters 2 and 3 were mutually exclusive to cluster 1, such that their appearances were transient in response to SNC and chronic upon DEN (Figures 2D and E). Based on this mutual exclusivity of the three clusters, we speculated that cluster 1 can sense and respond to nerve injuries, and that clusters 2 and 3 may have arisen from cluster 1 upon nerve injury.

To obtain clues on whether such changes between FAP clusters could have actually occurred in response to nerve injury, we first performed RNA velocity analysis using R package

267 velocyto.R (La Manno et al., 2018). RNA velocities on the UMAP plots predicted
268 transcriptomic flow from cluster 1 to clusters 2 and 3 in the early stages of regeneration in both
269 SNC- and DEN-affected FAPs, which was in line with our speculation (Figure 2—figure
270 supplement 1B). Conversely, transcriptomic flow from clusters 2 and 3 back to cluster 1 was
271 evident in SNC-affected FAPs in the later stages of regeneration (Figure 2—figure supplement
272 1B). However, RNA velocities in DEN-affected FAPs were represented as dots instead of
273 arrows on clusters 2 and 3 in the later stages, suggesting an unchanging, chronic state of their
274 transcriptomes, which is consistent with the chronic activation of FAPs in response to DEN
275 (Madaro et al., 2018) (Figure 2—figure supplement 1B). Additionally, hierarchical clustering
276 of the seven FAP clusters using DEGs enriched in each cluster grouped clusters 1-3 together,
277 supporting our speculation that clusters 2 and 3 originate from cluster 1 (Figure 2—figure
278 supplement 1C). Recently, *Hsd11b1*-expressing FAPs were identified as the FAP subset that is
279 specifically activated in response to nerve transection injury (Leinroth et al., 2022). Since we
280 speculated that cluster 1 in our scRNA-seq data can sense and respond to nerve injury, we
281 examined the expressions of marker genes identified in the previous report – *Hsd11b1*, *Mme*,
282 *Ret*, and *Gfra1* (Leinroth et al., 2022) – in our scRNA-seq data. Indeed, all four markers were
283 enriched in cluster 1 in our data (Figures 3A and B, Figure 2—figure supplements 1D–F).
284 Expressions of marker genes *Hsd11b1* and *Mme* were also enriched in clusters 2 and 3, further
285 supporting the idea that those clusters may have arisen from cluster 1 (Figure 2—figure
286 supplements 1D–F). Together, these data suggest that clusters 1-3 are the dynamic
287 interchanging subsets of FAPs that specifically respond to nerve injury, where cluster 1 senses
288 nerve injuries in unperturbed muscles and clusters 2 and 3 arise from cluster 1 to respond to
289 nerve injury.

290

291 **GDNF signaling pathway in the nerve injury-sensing mechanism by FAPs**

292 Among the four marker genes expressed in cluster 1, *Ret* and *Gfra1* are well-known as GDNF
293 receptors, where GFRα1 directly binds GDNF, which in turn activates the RTK RET for
294 downstream signal transduction (Jing et al., 1996; Treanor et al., 1996; Trupp et al., 1996).
295 Meanwhile, robust but specific expression of GDNF by Schwann cells in response to peripheral
296 nerve injury has been reported (Hammarberg et al., 1996; Hoke et al., 2002; Arthur-Farraj et
297 al., 2012; Xu et al., 2013; Proietti et al., 2021). Accordingly, we presumed that FAPs, especially
298 the *Ret*- and *Gfra1*-expressing cluster 1 cells, may sense the distant nerve injury by detecting
299 GDNF secreted from Schwann cells. Notably, both *Ret* and *Gfra1* were among the top 10 DEGs
300 specifically enriched in cluster 1, suggesting that they can readily respond to GDNF (Figure
301 2C, Figure 3—figure supplement 1A). In addition, comparing the expression levels of *Ret* and
302 *Gfra1* in skeletal muscle-resident mononuclear cell populations isolated by fluorescence-
303 activated cell sorting (FACS) revealed robust co-expression of both genes in FAPs, but not as
304 much in other cell populations (Figures 3C and D). Thus, FAPs may be the main cell type
305 within skeletal muscle that can respond to GDNF secreted by Schwann cells in case of a nerve
306 injury.

307

308 To further investigate the relevance of GDNF signaling in the nerve injury-sensing mechanism
309 by FAPs, we subjected lists of DEGs enriched in clusters 1-3 to ORA. Genes enriched in cluster
310 1 returned pathways 'GDNF receptor signaling pathway', 'regulation of cellular response to
311 growth factor stimulus', and 'positive regulation of peptidyl-tyrosine phosphorylation', where
312 tyrosine residues on the RTK RET is known to be phosphorylated upon activation (Jing et al.,

313 1996; Treanor et al., 1996; Trupp et al., 1996) (Figure 3—figure supplement 1B). The two latter
314 pathways were also found in the ORA results using DEGs enriched in clusters 2 and 3,
315 supporting the idea that those clusters originate from cluster 1 upon nerve injury (Figure 3E,
316 Figure 3—figure supplements 2A and B). The pathway 'positive regulation of ERK1/2 cascade'
317 was enriched in cluster 2, suggesting the involvement of GDNF-RET-Ras-ERK signaling
318 cascade within the MAPK signaling pathway in this cluster, which is one of the known
319 downstream pathways of canonical GDNF signaling (Airaksinen and Saarma, 2002; Sariola
320 and Saarma, 2003; Kanehisa et al., 2023) (Figure 3G, Figure 3—figure supplements 1C and
321 2A). In addition to ORA, we predicted upstream transcription factors (TFs) that could have
322 regulated the expressions of the DEGs enriched in the two activated FAP subsets, clusters 2
323 and 3, using TRRUST (Han et al., 2018). As a result, TFs *Fos*, *Jun* and *NF-κB* (*Nfkb1, Nfkb2*)
324 were predicted from both lists of DEGs, all of which are known to act downstream of the
325 GDNF/RET-induced MAPK signaling pathway (Fielder et al., 2018; Kanehisa et al., 2023)
326 (Figures 3F and G, Figure 3—figure supplement 1C, Supplemental tables 1 and 2). Collectively,
327 robust and specific co-expression of GDNF receptors in cluster 1, together with the prediction
328 of RTK activation and involvement of GDNF signaling pathway downstream TFs in clusters 2
329 and 3, suggests that GDNF signaling could be the mechanism by which FAPs sense the distant
330 nerve injury, where local Schwann cells act as the GDNF source upon nerve injury.

331

332 **The GDNF-BDNF axis as FAP's response mechanism to nerve injury**

333 Next, to discover how FAPs may contribute to nerve regeneration, we screened the list of genes
334 enriched in clusters 2 and 3 that were predicted to be downstream of the GDNF signaling
335 pathway to identify candidate effector genes. From the TRRUST analysis results, 44 genes

336 were identified to be regulated by either *Fos*, *Jun*, or *NF-κB* (Figure 4A, Supplemental tables
337 1–3). Since FAPs themselves do not constitute the neural components within skeletal muscle,
338 we reasoned that secreted factors from FAPs would most likely exert beneficial effect on the
339 regenerating nerves. Also, considering the effector gene's potential function in supporting
340 nerve regeneration, we presumed that it regulates neurons or glial cells. Moreover, we
341 anticipated that expression of the effector gene would be limited to the context of nerve injury
342 and regeneration, since the vast majority of FAPs are in a quiescent state in unperturbed adult
343 muscles (Scott et al., 2019). Thus, we applied the following criteria to narrow down our
344 candidate gene list: (1) genes that are known to code secreted proteins, (2) genes that are known
345 to regulate neurons or glial cells, and (3) genes that are expressed exclusively in activated FAPs
346 in response to nerve injury (Figure 4A, Supplemental table 3). Unexpectedly, after filtering out
347 genes that did not fit the three criteria, only *Bdnf* remained in our candidate gene list that could
348 act as the effector secreted by FAPs upon nerve injury to support nerve regeneration (Figure
349 4A). Expression patterns of *Bdnf* in FAPs upon nerve injury showed transient upregulation in
350 SNC-affected FAPs, whereas chronic expression of *Bdnf* was observed in DEN-affected FAPs,
351 showing correlation with its potential requirement during nerve regeneration (Figure 4C). The
352 expression of *Bdnf* was mostly limited to cluster 2 (Figure 4B), where pathway analysis and
353 TF prediction suggested the involvement of GDNF-RET-Ras-ERK-Fos signaling cascade in
354 this subset of FAPs (Figures 3F and G, Figure 3—figure supplements 1C and 2A). Accordingly,
355 we hypothesized that FAPs secrete BDNF in response to GDNF from Schwann cells upon
356 nerve injury, to actively take part in the regeneration process.

357

358 To validate our hypothesis *in vivo*, we first examined the expression profiles of *Gdnf* in
359 Schwann cells and *Bdnf* in FAPs at early time points in response to SNC, using $Plp1^{CreER}$;
360 $Rosa^{tdTomato}$ mice to specifically label and hence isolate Schwann cells (Doerflinger et al., 2003)
361 (Figure 4D). Expectedly, we could observe sequential upregulation of *Gdnf* and *Bdnf* from
362 Schwann cells and FAPs, respectively, where *Gdnf* levels peaked at 1 dpi in Schwann cells,
363 followed by a gradual increase of *Bdnf* expression in FAPs, which peaked at 3 dpi (Figures 4D
364 and E). Following mRNA expression validation *in vivo*, we performed western blot analysis
365 using FAPs isolated from either SNC-affected muscles at 7 dpi or from the contralateral,
366 uninjured muscles to validate the expression of BDNF protein upon nerve injury (Figure 4—
367 figure supplement 1). FAPs from both uninjured muscles and SNC-affected muscles showed
368 robust expression of PDGFRα, a well-known marker for FAPs (Joe et al., 2010; Uezumi et al.,
369 2010), indicating successful isolation and protein extraction from the sorted FAPs (Figure 4F).
370 However, unlike PDGFRα, the mature form of BDNF protein could only be detected in SNC-
371 affected FAPs, but not in uninjured FAPs, showing correlative results with the mRNA
372 expression pattern of *Bdnf* in FAPs upon nerve injury (Figures 4E and F). These results
373 demonstrate the expression of BDNF in nerve injury-affected FAPs, but not in uninjured FAPs,
374 on both mRNA and protein levels.

375

376 Next, to validate the sufficiency of GDNF signaling in inducing *Bdnf* expression in FAPs *in*
377 *vivo*, we injected recombinant mouse GDNF protein into the TA and the two gastrocnemius
378 (GA) muscles (lateral and medial GA), from which FAPs were FACS-isolated 48 hours post
379 injection to investigate the expression of *Bdnf* (Figure 4G). Compared to PBS control,
380 intramuscular injection of GDNF sufficiently induced *Bdnf* expression in FAPs, even in the

absence of a nerve injury (Figures 4G and H). Conversely, to show the necessity of GDNF signaling in the upregulation of *Bdnf* in FAPs upon nerve injury, we injected either IgG control or anti-GDNF antibodies into the TA and GA muscles 24 hours after SNC, and FACS-isolated FAPs 48 hours post injection for analysis. Though the results were not statistically significant, injection of GDNF blocking antibodies showed a tendency to reduce *Bdnf* expression compared to IgG-injected controls, which is in support of our hypothesis (Figure 4—figure supplement 2). Together, we suggest that FAPs can respond to nerve injury via the GDNF-BDNF axis, since recombinant GDNF protein could sufficiently induce *Bdnf* expression in FAPs without nerve injury, and reduced GDNF activity could weaken *Bdnf* expression in the nerve injury-affected FAPs.

Remyelination by FAP-derived BDNF during peripheral nerve regeneration

Although BDNF is known to function in processes such as axon elongation (Oudega and Hagg, 1999; English et al., 2013), survival of neurons (Ghosh et al., 1994; Baydyuk and Xu, 2014), and myelination by Schwann cells (Zhang et al., 2000; Chan et al., 2001; Xiao et al., 2009), the role of BDNF secreted by FAPs in nerve regeneration is unknown. To find out how FAP-derived BDNF can contribute to nerve regeneration, we produced conditional knockout (cKO) mice where *Bdnf* is specifically inactivated in mesenchymal progenitors including FAPs, by crossing $Prrx1^{Cre}$ mice (Logan et al., 2002; Kim et al., 2022; Leinroth et al., 2022; Hann et al., 2024) with *Bdnf*-floxed ($Bdnf^{fl}$) mice ($Prrx1^{Cre}$; $Bdnf^{fl/fl}$, hereafter cKO) (Figure 5—figure supplement 1A). Inactivation of *Bdnf* in FAPs in the cKO mice was confirmed on both genomic DNA and mRNA levels (Figure 5—figure supplements 1B and C). Though Cre expression in *Prrx1*-expressing cells occur from embryonic day 9.5 (Logan et al., 2002), no visible

404 phenotypes were observed in the postnatal, juvenile and adult cKO mice compared to littermate
405 controls (hereafter, Ctrl). However, upon SNC in the right hindlimb, cKO mice displayed a
406 delay in nerve regeneration compared to Ctrl, measured by compound muscle action potential
407 (CMAP) amplitude and latency via electromyography (EMG) on the GA muscle (Figures 5A–
408 5D, Figure 5—figure supplements 1D and E). At 4 weeks post injury (wpi), nerve regeneration
409 in both Ctrl and cKO mice showed insufficient recovery in the right, injured GA compared to
410 the left, uninjured GA, where lower amplitude and prolonged latency in CMAP was observed
411 (Figures 5B–D). However, at 6 wpi, while CMAP amplitude and latency in the left and right
412 GAs became comparable in Ctrl mice, recovery of such values were stalled at levels
413 comparable to 4 wpi in the cKO mice (Figures 5B–D). By 12 wpi, electrophysiological
414 functions of the injured nerves became statistically comparable to that of its contralateral
415 counterpart in the cKO mice, indicating a delayed regeneration in the cKO mice (Figures 5B–
416 D).

417

418 Generally, decrease in CMAP amplitude and prolonged CMAP latency can be explained by
419 two main causes: axonal loss and defective myelination (Mallik and Weir, 2005; Chung et al.,
420 2014). Since complete regeneration of the injured nerves on the electrophysiological level
421 could be achieved after a sufficient period of time in the cKO mice (Figures 5B–D), we
422 presumed that axonal loss would not have occurred, since it would result in permanent defects
423 by loss of motor units. Instead, we thought that defective myelination could have occurred in
424 the cKO mice, considering the fact that BDNF is already known to promote remyelination
425 during peripheral nerve regeneration (Zhang et al., 2000; Chan et al., 2001; Zheng et al., 2016),
426 and that defective myelination alone can affect both CMAP amplitude and latency (Mallik and

427 Weir, 2005). Thus, we investigated the effect of conditional *Bdnf* inactivation in FAPs on
428 regenerative myelination by examining the sciatic nerves from Ctrl versus cKO mice at 6 wpi,
429 when the delayed functional recovery of the injured nerves in the cKO mice was prominent
430 (Figures 5A–D). Toluidine blue staining of the semi-thin sections of injured sciatic nerves
431 revealed significantly reduced myelin thickness in the cKO mice compared to Ctrl mice (Figure
432 5E). Indeed, higher G-ratio values were calculated from cKO mice compared to Ctrl,
433 confirming the reduced myelination in the regenerating nerves in cKO mice (Figure 5F, Figure
434 5—figure supplements 1F–H). This decrease in myelin thickness was independent from axon
435 diameter, which were comparable in both Ctrl and cKO mice, implying that no axonal loss or
436 defect had occurred in the cKO mice compared to controls (Figure 5G). Taken together, our
437 results revealed the direct involvement of FAP-derived BDNF in the remyelination process
438 during peripheral nerve regeneration, such that inadequate levels of *Bdnf* expression in FAPs
439 caused delayed remyelination and hence delayed nerve regeneration in the cKO mice.

440

441 **Implication of FAP-derived BDNF in the age-related delay in nerve regeneration**

442 Finally, to seek clinical relevance of *Bdnf* expression in FAPs during nerve regeneration, we
443 compared the expression levels of *Bdnf* in adult (5-6 months) versus aged (24 months) mice in
444 FAPs post SNC. At 7 dpi, *Bdnf* expression was significantly reduced in the aged mice compared
445 to adult mice (Figures 6A and B). Such a difference could be one of the factors that lead to the
446 delayed or failed regeneration of injured nerves in the elderly compared to healthy, young
447 adults, suggesting the clinical role of FAPs in a timely, successful peripheral nerve regeneration
448 process.

449

450 **Discussion**

451 Traumatic injury to the peripheral nerve has severe consequences, including lifelong paralysis
452 of the injured limb that can compromise the quality of life significantly (Grinsell and Keating,
453 2014). Thus, understanding the regeneration process of the peripheral nerves is fundamental
454 for treating the potentially devastating injury. Previously, several cellular components in and
455 outside the injured nerve were discovered to actively participate in the regeneration process,
456 including the injured neurons (Hanz et al., 2003), glial cells (Arthur-Farraj et al., 2012),
457 immune cells (Mueller et al., 2001; Kalinski et al., 2020), and nerve-resident mesenchymal
458 cells (Parrinello et al., 2010; Toma et al., 2020), via diverse mechanisms so that the nerve can
459 regain its function (Scheib and Hoke, 2013). In this study, we investigated the response
460 mechanism of muscle-resident FAPs to both acute and chronic peripheral nerve injury via
461 scRNA-seq, and revealed that this population of cells can also actively take part in the nerve
462 regeneration process. Here, we discovered that muscle-resident FAPs can recognize the distant
463 nerve injury by sensing GDNF secreted by Schwann cells. Though GDNF secretion by
464 Schwann cells in response to nerve injury had previously been recognized (Hammarberg et al.,
465 1996; Hoke et al., 2002; Arthur-Farraj et al., 2012; Xu et al., 2013; Proietti et al., 2021), we
466 identified FAPs as a major target cell population of GDNF within skeletal muscle, based on the
467 enriched expression of GDNF receptors. In depth, exploiting the technical advantage of
468 scRNA-seq, we suggested that a subset of FAPs, named cluster 1 in this study, can sense the
469 local GDNF by expressing GDNF receptors *Ret* and *Gfra1*, and that upon GDNF sensing,
470 cluster 1 FAPs turn into clusters 2 and 3 to contribute to the nerve regeneration process.
471 Specifically, we discovered that FAPs, especially the *F2rl1*-expressing cluster 2, express *Bdnf*
472 in response to nerve injury and/or GDNF, which in turn was shown to promote the

473 remyelination process by Schwann cells during nerve regeneration, using our cKO mouse
474 model (Figure 6C). Since epineurial and perineurial, but not endoneurial mesenchymal cells
475 share their origins with the muscle-resident FAPs and therefore are *Prrx1*-positive (Joseph et
476 al., 2004; Carr et al., 2019), the possibility that the delayed remyelination observed in our cKO
477 mice could be due to the combined effect of *Bdnf* depletion in both muscle- and nerve-resident
478 mesenchymal cells cannot be eliminated. To resolve such issue, further investigations using
479 muscle-resident FAP-specific Cre mouse lines is required, but such line is currently unavailable
480 as no such specific marker has been found. Nevertheless, our findings show that muscle-
481 resident FAP-derived BDNF is indeed important for nerve regeneration, since intramuscular
482 injection of recombinant BDNF can sufficiently accelerate the nerve regeneration process
483 (Zheng et al., 2016). Conversely, intramuscular injection of BDNF-neutralizing antibodies can
484 sufficiently delay nerve regeneration (Zheng et al., 2016). Thus, endogenous supply of
485 intramuscular BDNF by the muscle-resident FAPs in our Ctrl mice would likely have supported
486 remyelination by Schwann cells, while the lack of such BDNF supply by FAPs in our cKO
487 mice would have resulted in delayed remyelination. Also, we found that while muscle-resident
488 FAPs robustly express both GDNF receptor genes, neither epineurial nor perineurial
489 mesenchymal cells express significant levels of *Ret* and *Gfra1* (Carr et al., 2019; Toma et al.,
490 2020; Zhao et al., 2022) (Supplemental figure 1), implying that the GDNF-BDNF axis found
491 in this study could be valid uniquely in muscle-resident FAPs. Collectively, we suggest that
492 muscle-resident mesenchymal progenitors can directly contribute to nerve regeneration via the
493 GDNF-BDNF axis (Figure 6C), of which was previously unidentified; we suggest that in future
494 studies regarding peripheral nerve regeneration, active participation of this intramuscular
495 mesenchymal population should be taken into consideration. In that process, our scRNA-seq
496 data may provide valuable insights, which may lead to additional discoveries on FAP's

contributions to nerve regeneration by other mechanisms, and/or provide clues on the cell-to-cell communications of FAPs with other cell types that may lead to facilitation of the regeneration process.

Here, we have primarily investigated the roles of *Ret*-expressing and *F2rl1*-expressing FAPs in sensing and responding to nerve injury, respectively. However, possibilities that other subpopulations can exert distinct beneficial effects on nerve regeneration remain largely unexplored. For example, although identified as a nerve injury-relevant subpopulation in this study, specific contributions of the *Alkal2*-expressing cluster 3 FAPs to nerve regeneration are yet to be discovered. Identification of effector genes such as *Bdnf* from this subpopulation may lead to the discovery of an additional mechanism by which FAPs can contribute to nerve regeneration. Although other subpopulations (clusters 4-7) did not exhibit dramatic fluctuations in population percentage, some of the genes expressed specifically in those subpopulations showed patterns that followed the regeneration process (Supplemental figure 2). Such gene expression patterns suggest subpopulation-specific functions even in the less dynamic subpopulations within FAPs in peripheral nerve regeneration, and require further investigations to reveal their possible contributions.

The role of BDNF in peripheral nerve regeneration has been identified previously, where it was found to promote both intrinsic axonal regeneration in neurons as well as remyelination by Schwann cells (Zhang et al., 2000; Chan et al., 2001; Zheng et al., 2016). In such circumstances, various cellular sources of BDNF have been identified. Bone marrow transplantation of wild-type cells into *Bdnf* heterozygotic knockout mice revealed the involvement of bone marrow-

520 derived cells in expressing *Bdnf* that can promote nerve regeneration in the sciatic nerve
521 (Takemura et al., 2012). Schwann cells themselves are cellular sources of BDNF during nerve
522 regeneration (Wilhelm et al., 2012). In this study, we showed that BDNF from FAPs can also
523 promote myelination of the regenerating axons post injury, suggesting FAPs as an additional
524 cellular source of BDNF in peripheral nerve regeneration. The existence of cellular sources of
525 BDNF other than FAPs such as Schwann cells would provide an explanation for the delayed,
526 but not failed, remyelination in our *Bdnf* cKO mice, where complete regeneration had occurred
527 after a sufficient amount of time, despite the lack of *Bdnf* expression in FAPs. Still, ablation of
528 *Bdnf* in FAPs displayed significant delays in the remyelination process during nerve
529 regeneration, suggesting their requirement in the timely regeneration process of injured nerves.
530 Meanwhile, scRNA-seq data of all mononuclear cells from denervated muscles (Nicoletti et
531 al., 2023) suggested expression of *Bdnf* in tenocytes and pericytes in addition to Schwann cells
532 and FAPs (Supplemental figures 3A and B). Although this may imply the involvement of those
533 cellular components in providing BDNF for nerve regeneration, expression of *Bdnf* in such
534 cells were not altered as significantly in response to nerve injury as in FAPs or Schwann cells
535 (Supplemental figure 3C). Moreover, while *Ret*-expressing FAPs and Schwann cells are known
536 to be in proximity to the NMJ or relevant nerve regeneration sites (Leinroth et al., 2022), such
537 locational enrichment of tenocytes and pericytes have not been reported so far. Thus, it is likely
538 that FAPs, together with Schwann cells, are the main sources of BDNF within skeletal muscle
539 that can act in the remyelination process during peripheral nerve regeneration.

540

541 Aging is one of the well-known factors that can slow down the nerve regeneration process
542 (Verdú et al., 2008; Maita et al., 2023). Since multiple cell types are known to participate in

543 this process (Scheib and Hoke, 2013), determination of the cell types that can cause age-related
544 delays in nerve regeneration is important for the development of therapeutic approaches
545 targeting the relevant cell types. Of note, previous research emphasized the importance of niche
546 factors, rather than the intrinsic regenerative capacity of the injured neurons, in the age-related
547 decline in nerve regeneration (Painter et al., 2014). Specifically, inability of Schwann cells to
548 adopt repair cell phenotypes has been pointed out as one of the age-related changes (Painter et
549 al., 2014; Wagstaff et al., 2021). In addition, age-related changes in immune cells, especially
550 macrophages, were suggested as causal factors that delay nerve regeneration (Buttner et al.,
551 2018). In particular, chronic inflammatory phenotypes were shown to interfere with the
552 remyelination process by Schwann cells (Buttner et al., 2018), and failed macrophage
553 infiltration in the early stages of regeneration resulted in defective Wallerian degeneration and
554 myelin debris clearing (Scheib and Hoke, 2016). In addition to the involvement of Schwann
555 cells and immune cells, we have identified muscle-resident FAPs as an additional cellular
556 component that can contribute to nerve regeneration, by promoting remyelination via BDNF
557 secretion. Surprisingly, expression of *Bdnf* by FAPs was significantly reduced in aged mice
558 compared to adult mice, suggesting the clinical relevance of FAP's involvement in the age-
559 related delay in peripheral nerve regeneration. We believe that further studies on age-related
560 changes in FAPs may provide valuable clues to understanding clinical observations from aged
561 individuals, which can lead to development of additional therapeutic strategies that include
562 FAPs as target cells in treating both young and aged nerve injury patients.

563

564 **Materials and Methods**

565

566 ***Animals***

567 C57BL/6J (RRID:IMSR_JAX:000664), *Prrx1*^{Cre} (RRID:IMSR_JAX:005584), *Bdnf*^{fl}
568 (RRID:IMSR_JAX:004339), *Plp1*^{CreER} (RRID:IMSR_JAX:005975) and *Rosa*^{tdTomato}
569 (RRID:IMSR_JAX:007914) mice were all obtained from The Jackson Laboratory. To generate
570 *Prrx1*^{Cre}; *Bdnf*$^{fl/fl}$ mice, *Prrx1*$^{Cre/+}$; *Bdnf*$^{fl/+}$ males and *Bdnf*$^{fl/fl}$ females were crossed to avoid
571 germline recombination in the female reproductive cells, and littermates were used as controls.
572 To generate *Plp1*^{CreER}; *Rosa*^{tdTomato} mice, *Plp1*$^{CreER/+}$ mice were crossed with *Rosa*$^{tdTomato/+}$ mice,
573 and the line was kept by breeding *Plp1*$^{CreER/+}$; *Rosa*$^{tdTomato/tdTomato}$ males and females. Only mice
574 that had the *Plp1*^{CreER} allele was used. Primers used for genotyping are listed in Supplemental
575 table 4. All mice were bred on the B6 background, except for the *Prrx1*^{Cre}; *Bdnf*$^{fl/fl}$ mice and
576 littermates that were kept in the mixed B6, 129S4 and BALB/c background. All mice were
577 housed in a specific-pathogen-free (SPF) animal facility, with 12-h light/12-h dark cycle at
578 room temperature (RT, 22°C) and 40~60% humidity, and were fed with normal chow diet and
579 water ad libitum. Tamoxifen administration, sciatic nerve crush injury, denervation, and
580 intramuscular injection of GDNF or GDNF blocking antibodies were all given to 3 to 4-month-
581 old adult mice. When comparing aged mice versus adult mice, 24-month-old and 5 to 6-month-
582 old mice were used, respectively. In all cases except for *Plp1*^{CreER}; *Rosa*^{tdTomato} mice, male mice
583 were used for the experiments. No sex-specific differences were observed in experiments using
584 *Plp1*^{CreER}; *Rosa*^{tdTomato} mice. All experimental procedures were approved by the Institutional
585 Animal Care and Use Committtee at Seoul National University and were carried out according
586 to the guidelines provided.

587

588 ***Tamoxifen administration***

589 To label Schwann cells, 3-month-old *Plp1*^{CreER}; *Rosa*^{tdTomato} mice were administered orally with
590 tamoxifen (20 mg/ml in corn oil, 160 mg/kg body weight; Sigma-Aldrich) 3 times every other
591 day.

592

593 ***Sciatic nerve injury***

594 Mice were deeply anesthesized via intraperitoneal injection of Avertin (32 mg/ml, ~800 mg/kg;
595 Sigma-Aldrich), and the incision site on the posterior side of the right hindlimb was shaved
596 and depilated using surgical clippers and hair removal cream. After cleansing the incision site
597 with 70% ethanol, incision was made on the skin with surgical scissors and the biceps femoris
598 muscle was punctured open with fine-tip forceps to expose the sciatic nerve. For sciatic nerve
599 crush injury, the exposed nerve was crushed with fine forceps for 30 seconds at the site just
600 proximal to where the tibial, peroneal and sural nerves branched out from the sciatic nerve. For
601 denervation, ~5 mm of the sciatic nerve proximal from the crush injury site was cut and
602 removed. The punctured biceps femoris muscle and skin were then sutured, and the incision
603 site was sterilized with povidion-iodine.

604

605 ***Intramuscular injection of GDNF***

606 Tibialis anterior muscle and the two gastrocnemius muscles (GA, lateral and medial) were each
607 injected with 10 μl of either PBS or recombinant mouse GDNF (10 μg/ml, Sigma-Aldrich)
608 using 31-gauge insulin syringes without damaging any innervating nerves. The injected
609 muscles were then dissected 48 hours post injection for isolation of FAPs and further analysis.

610

611 ***Intramuscular injection of GDNF blocking antibodies***

612 Tibialis anterior muscle and the two gastrocnemius muscles (GA, lateral and medial) were each
613 injected with 10 μg of either normal rabbit IgG (Sino Biological) or anti-GDNF antibodies
614 (Alomone Labs) using 31-gauge insulin syringes 24 hours post SNC. The injected muscles
615 were then dissected 48 hours post injection (72 hours post injury) for isolation of FAPs and
616 further analysis.

617

618 ***Isolation of FAPs, Schwann cells and others***

619 Isolation of muscle-resident FAPs, Schwann cells and others was performed according to a
620 previously reported protocol (Liu et al., 2015) with minor modifications. Muscles indicated in
621 each experiment were dissected, finely chopped with surgical scissors and washed with 10%
622 horse serum (Gibco), DMEM (HyClone) for further dissociation. Enzymatic dissociation was
623 carried out in 10% horse serum, DMEM containing collagenase II (800 U/ml, Worthington
624 Biochemical) and dispase II (1.1 U/ml, Gibco) for 40 minutes at 37°C with mild agitation, and
625 mechanical dissociation was performed by tituration of the dissociated solution with a 20-
626 gauge needle ten times. After filtering the solution through a 40 μm strainer, dissociated
627 mononuclear single cells were stained with the following antibodies: APC anti-mouse CD31,
628 APC anti-mouse CD45, PE anti-mouse TER-119, biotin anti-mouse CD106 (Vcam1)
629 (Biolegend) and FITC anti-mouse Ly-6A/E (Sca1) (BD Pharmingen). 7-aminoactinomycin D
630 (7-AAD, Sigma-Aldrich) was added to stain dead cells, and PE/Cy7 streptavidin was used to
631 label Vcam1^{+} cells. Gating strategies used for the isolation of each cell type were as follows:
632 FAPs, 7-AAD^{-}Ter119^{-}CD31^{-}CD45^{-}Vcam1^{-}Sca1^{+}; MuSCs, 7-AAD^{-}Ter119^{-}CD31^{-}CD45^{-}
633 Vcam1^{+}Sca1^{-}; lineage-positive cells, 7-AAD^{-}Ter119^{-}CD31^{+} or 7-AAD^{-}Ter119^{-}CD45^{+}; double-

634 negative cells, 7-AAD$^-$Ter119$^-$CD31$^-$CD45$^-$Vcam1$^-$Sca1$^-$. For Schwann cells, 7-AAD$^-$
635 tdTomato$^+$ cells were sorted from tamoxifen-administered *Plp1*^{CreER}; *Rosa*^{tdTomato} mice.

636

637 ***scRNA-seq library construction and sequencing***

638 FAPs were isolated from sciatic nerve crush injury-affected or denervated muscles on days 3,
639 7, 14 and 28 post injury using wild type B6 mice, so that a total of nine samples, including
640 uninjured control, were collected for library generation. For each sample, isolated FAPs were
641 pooled from two mice. Chromium Next GEM Single Cell 3′ Kit v3.1 (10x Genomics) was used
642 according to the manufacturer's instructions for the nine collected FAP samples, and target cell
643 number for recovery was set to 5,000 in each sample. Sequencing of the libraries was carried
644 out using HiSeq X Ten (Illumina).

645

646 ***Computational analysis of scRNA-seq data***

647 Sequenced reads were aligned to the mouse reference genome mm10 using CellRanger v3.1.0
648 (10x Genomics), and aligned reads were transformed into gene-cell count matrices using
649 velocyto v0.17 (La Manno et al., 2018) to obtain count matrices for both spliced and unspliced
650 mRNAs. Output loom files were then loaded with R package SeuratWrappers v0.3.1, and were
651 preprocessed and analyzed using R package Seurat v4.3.0 (Hao et al., 2021) for downstream
652 analysis. The preprocessing steps for quality control included doublet filtering, live cell
653 filtering and removal of non-FAPs as previously described (Kim et al., 2022). All nine sample
654 data were merged and normalized for dimensionality reduction, where top 8 principal
655 components from the principal component analysis using 5,000 variable genes were selected

656 for 2-dimensional UMAP embedding and visualization. Unsupervised clustering of cells was
657 achieved through FindNeighbors and FindClusters functions in Seurat R package. To identify
658 DEGs in the pairwise comparisons of scRNA-seq samples, the FindMarkers function in Seurat
659 R package was used with the following parameters: fold change >= 2, pseudocount.use = 0.01,
660 min.pct = 0.01, adjusted p value < 0.05. For identification of DEGs in each cluster,
661 FindAllMarkers function was used with the parameters: fold change >= 1.5, pseudocount.use
662 = 0.01, min.pct = 0.02, adjusted p value < 0.05. For hierarchical clustering, R package
663 pheatmap v1.0.12 was used. For RNA velocity analysis, R package velocyto.R v0.6 was used
664 following the instructions provided by the developer (La Manno et al., 2018). For the prediction
665 of upstream regulatory transcription factors using lists of DEGs enriched in the selected FAP
666 clusters, the web-based tool TRRUST v2 (Han et al., 2018) was used. For color mapping of the
667 MAPK signaling pathway, online version of the KEGG Mapper – Color (Kanehisa et al., 2023)
668 was used.

669

670 ***Gene set overrepresentation analysis***

671 To identify pathways enriched in the lists of DEGs, web-based version of g:Profiler (Kolberg
672 et al., 2023) was used with the following parameters: organism – Mus musculus; ordered query
673 – YES; data sources – GO biological process without electronic GO annotations, Reactome,
674 and WikiPathways; advanced options were set to default. Visualization of the results were done
675 as previously described (Reimand et al., 2019), using the Cytoscape v3.10.1 (Shannon et al.,
676 2003) application with tools EnrichmentMap v3.3.6 (Merico et al., 2010) and AutoAnnotate
677 v1.4.1 (Kucera et al., 2016).

678

679 ***RNA extraction and qRT-PCR***

680 Total RNA extraction and reverse transcription was carried out for isolated FAPs, Schwann
681 cells, MuSCs and others using TRIzol™ reagent (Invitrogen) and ReverTra Ace™ qPCR RT
682 Master Mix (Toyobo) reagents respectively, following the manufacturer's instructions. qPCR
683 was performed using ORA™ SEE qPCR Green ROX L Mix (HighQu) reagent, with gene-
684 specific primers listed in Supplemental table 4. Quantitative analysis of mRNA levels were
685 done using the $2^{-\Delta\Delta Ct}$ method with β-actin (*Actb*) as the housekeeping gene for normalization.

686

687 ***Western blot analysis***

688 FACS-isolated FAPs were lysed in RIPA buffer (Biosesang) added with 1x Halt protease
689 inhibitor cocktail (Thermo Scientific), and were sonicated. The lysate was then centrifuged at
690 13,000 rpm for 30 minutes at 4°C, and the supernatant was mixed with Laemmli sample buffer
691 before heating at 95°C for 10 minutes. Samples were subjected to electrophoresis in 10%
692 polyacrylamide gels and transferred to 0.45 μm PVDF membranes (Immobilon). For GAPDH
693 (rabbit anti-GAPDH, 1:1000, Bethyl Laboratories) and PDGFRα (rabbit anti-PDGFRα, 1:200,
694 Santa Cruz Biotechnology), membranes were blocked in 5% skim milk (LPS Solution), 0.1%
695 Tween-20 (Sigma-Aldrich) in TBS, and incubated with primary antibodies overnight at 4°C,
696 and then with the secondary antibody (horseradish peroxidase-conjugated anti-rabbit IgG,
697 1:10,000, Promega) for 1 hour at RT. For BDNF (rabbit anti-BDNF, 1:1000, Alomone Labs),
698 membranes were blocked in 5% bovine serum albumin (Bovogen Biologicals), 0.1% Tween-
699 20 in TBS, and incubated with the primary antibody in immunoreaction enhancer solution 1
700 (Toyobo) for 1 hour at RT, and then with the same secondary antibody in immunoreaction
701 enhancer solution 2 (Toyobo) for 1 hour at RT. The membranes were then developed using

702 SuperSignal West Dura Extended Duration Substrate (Thermo Scientific) according to the
703 manufacturer's instructions, and imaged with FUSION Solo chemiluminescence imaging
704 system (Vilber Lourmat). Densitometric quantification of the imaged data were performed
705 using ImageJ v1.51n (NIH).

706

707 ***Electromyography and CMAP measurement***

708 Intraperitoneal injection of Avertin (32 mg/ml, ~800 mg/kg) for anesthetization of mice was
709 carried out prior to CMAP measurement. Stimulation of the sciatic nerve was achieved by
710 placing stimulating electrodes subcutaneously on either side of the sciatic notch and applying
711 supramaximal stimuli (~70 mA) at a rate of 1 pulse per second with the duration of 0.1 ms,
712 using Isolated Pulse Stimulator Model 2100 (A-M Systems). Recording electrode was placed
713 carefully on the GA muscle subdermally without puncturing the muscle, with the reference
714 electrode placed near the Achilles tendon and ground electrode placed on the tail for data
715 recording using Data Recorder IX-RA-834 (iWorx). CMAP amplitude was determined by the
716 absolute difference between potentials of positive and negative peaks, and CMAP latency was
717 determined by the delay from stimulus peak to the beginning of response peak. Three individual
718 measurements were taken from each animal's GA muscle, and average values were used as
719 representatives for statistical analysis.

720

721 ***Toluidine blue staining of sciatic nerves***

722 Sciatic nerve distal to the injury site was dissected at 6 weeks post injury for analysis. The
723 dissected nerves were fixed in 4% paraformaldehyde dissolved in Sorensen's phosphate buffer

724 (0.1M, pH 7.2) at 4°C overnight, followed by procedures described previously (Kim et al.,
725 2022) with minor modifications for semi-thin sectioning. Briefly, fixed samples were washed
726 with 0.1M sodium cacodylate buffer (pH 7.2), post-fixed with 1% osmium tetroxide in 0.1M
727 sodium cacodylate buffer (pH 7.2) for 1 hour at RT, washed with distilled water (DW) and
728 stained with 0.5% uranyl acetate at 4°C overnight. Stained samples were then washed with DW
729 and dehydrated using serial ethanol and propylene oxide. Samples were then embedded in
730 Spurr's resin (Electron Microscopy Sciences), and semi-thin sections (500 nm) were prepared
731 with a diamond knife on an ultramictorome EM UC7 (Leica). The sections were dried down
732 on glass slides for staining and light microscopy. Toluidine blue staining were done using 1%
733 toluidine blue solution containing 1% sodium borate on a slide warmer (70°C), and images
734 were obtained with the light microscope EVOS FL Auto 2 (Thermo Fisher Scientific) for
735 analysis.

736

737 ***G-ratio quantification***

738 Semi-automated quantification of naked and myelinated axon diameters were carried out using
739 an ImageJ plugin for g-ratio quantification (Goebbels et al., 2010), where axon diameters and
740 G-ratios were quantified and calculated, respectively. G-ratios were calculated as [naked axon
741 diameter]/[myelinated axon diameter].

742

743 ***Quantification and statistical analysis***

744 All statistical analyses were performed using Prism v5.01 (GraphPad) and R v4.2.1.
745 Continuous variables were tested for normal distribution with Shapiro-Wilk test, and F-test was

746 used to check for equal variance. For comparison of significant differences in multiple groups,
747 one-way analysis of variance (ANOVA) followed by Bonferroni's pairwise post hoc test was
748 applied. For comparison of two groups, unpaired t-test was used for data with normal
749 distribution and equal variance; Welch's t-test was used for data with normal distribution and
750 unequal variance; and Mann-Whitney U test was used for non-normally distributed data.
751 ANCOVA was applied to test for differences between slopes of linear regression lines. Two-
752 way ANOVA was applied to compare two groups with two variables. For comparison of gene
753 expression levels between scRNA-seq data, Wilcoxon rank sum test was applied as a default
754 in functions FindAllMarkers and FindMarkers within the R package Seurat v4.3.0. For RT-
755 qPCR, the average of triplicate technical values were used for each biological replicate. All
756 error bars represent mean ± SD. *P* value of less than 0.05 was considered statistically significant
757 at the 95% confidence level. The number of technical and biological replicates and statistical
758 analysis used in each experiment are indicated in the figure legends.

759

760 **Data availability**

761 Single-cell RNA-sequencing data produced in this study have been deposited at GEO under
762 accession number GSE250436 and are publicly available as of the date of publication.

763

764 **Acknowledgments**

765 We thank Dr. Jong-Eun Park for his helpful comments on the analysis of our scRNA-seq data.
766 *Prrx1*^{Cre} mice, *Bdnf*^{fl} mice, and *Plp1*^{CreER} mice were obtained via Korea Mouse Phenotyping
767 Center, deposited by Dr. Rho Hyun Seong, Dr. Yun-Hee Lee, and Dr. Myunghwan Choi,

respectively. Also, we would like to acknowledge technical support from Center for Research Facilities, Biological Sciences Department, Seoul National University (SNU) and SNU National Instrumentation Center for Environmental Management. Library construction and sequencing of the scRNA-seq data was performed by Macrogen Inc.. Experimental schemes and graphical summary in this paper were created using BioRender. This work was supported by grants from the National Research Foundation of Korea (NRF-2020R1A5A1018081, NRF-2022R1A2C3007621) funded by the Korean government (MSIT).

References

Airaksinen MS, and Saarma M (2002). **The GDNF family: signalling, biological functions and therapeutic value.** *Nat Rev Neurosci* 3:383-94.10.1038/nrn812

Arthur-Farraj PJ, Latouche M, Wilton DK, Quintes S, Chabrol E, Banerjee A, Woodhoo A, Jenkins B, Rahman M, Turmaine M, Wicher GK, Mitter R, Greensmith L, Behrens A, Raivich G, Mirsky R, and Jessen KR (2012). **c-Jun reprograms Schwann cells of injured nerves to generate a repair cell essential for regeneration.** *Neuron* 75:633-47.10.1016/j.neuron.2012.06.021

Aurora AB, and Olson EN (2014). **Immune modulation of stem cells and regeneration.** *Cell Stem Cell* 15:14-25.10.1016/j.stem.2014.06.009

Bakooshli MA, Wang YX, Monti E, Su S, Kraft P, Nalbandian M, Alexandrova L, Wheeler JR, Vogel H, and Blau HM (2023). **Regeneration of neuromuscular synapses after acute and chronic denervation by inhibiting the gerozyme 15-prostaglandin dehydrogenase.** *Science Translational Medicine* 15:eadg1485.doi:10.1126/scitranslmed.adg1485

Baydyuk M, and Xu B (2014). **BDNF signaling and survival of striatal neurons.** *Front Cell Neurosci* 8:254.10.3389/fncel.2014.00254

Buttner R, Schulz A, Reuter M, Akula AK, Mindos T, Carlstedt A, Riecken LB, Baader SL, Bauer R, and Morrison H (2018). **Inflammaging impairs peripheral nerve maintenance and regeneration.** *Aging Cell* 17:e12833.10.1111/acel.12833

Carr MJ, Toma JS, Johnston APW, Steadman PE, Yuzwa SA, Mahmud N, Frankland PW,

796 Kaplan DR, and Miller FD (2019). **Mesenchymal Precursor Cells in Adult Nerves**
797 **Contribute to Mammalian Tissue Repair and Regeneration.** *Cell Stem Cell* 24:240-256
798 e9.10.1016/j.stem.2018.10.024

799 Chan JR, Cosgaya JM, Wu YJ, and Shooter EM (2001). **Neurotrophins are key mediators of**
800 **the myelination program in the peripheral nervous system.** *Proceedings of the National*
801 *Academy of Sciences* 98:14661-14668.

802 Chung T, Prasad K, and Lloyd TE (2014). **Peripheral neuropathy: clinical and**
803 **electrophysiological considerations.** *Neuroimaging Clin N Am* 24:49-
804 65.10.1016/j.nic.2013.03.023

805 Cintron-Colon AF, Almeida-Alves G, Boynton AM, and Spitsbergen JM (2020). **GDNF**
806 **synthesis, signaling, and retrograde transport in motor neurons.** *Cell Tissue Res* 382:47-
807 56.10.1007/s00441-020-03287-6

808 Contreras O, Rebolledo DL, Oyarzun JE, Olguin HC, and Brandan E (2016). **Connective**
809 **tissue cells expressing fibro/adipogenic progenitor markers increase under chronic**
810 **damage: relevance in fibroblast-myofibroblast differentiation and skeletal muscle fibrosis.**
811 *Cell Tissue Res* 364:647-660.10.1007/s00441-015-2343-0

812 Contreras O, Rossi FMV, and Theret M (2021). **Origins, potency, and heterogeneity of**
813 **skeletal muscle fibro-adipogenic progenitors-time for new definitions.** *Skelet Muscle*
814 11:16.10.1186/s13395-021-00265-6

815 De Micheli AJ, Laurilliard EJ, Heinke CL, Ravichandran H, Fraczek P, Soueid-Baumgarten S,
816 De Vlaminck I, Elemento O, and Cosgrove BD (2020). **Single-Cell Analysis of the Muscle**
817 **Stem Cell Hierarchy Identifies Heterotypic Communication Signals Involved in Skeletal**
818 **Muscle Regeneration.** *Cell Rep* 30:3583-3595 e5.10.1016/j.celrep.2020.02.067

819 Doerflinger NH, Macklin WB, and Popko B (2003). **Inducible site-specific recombination in**
820 **myelinating cells.** *Genesis* 35:63-72.10.1002/gene.10154

821 Encinas M, Tansey MG, Tsui-Pierchala BA, Comella JX, Milbrandt J, and Johnson EM (2001).
822 **c-Src is required for glial cell line-derived neurotrophic factor (GDNF) family ligand-**
823 **mediated neuronal survival via a phosphatidylinositol-3 kinase (PI-3K)-dependent**
824 **pathway.** *Journal of Neuroscience* 21:1464-1472.

825 English AW, Liu K, Nicolini JM, Mulligan AM, and Ye K (2013). **Small-molecule trkB**
826 **agonists promote axon regeneration in cut peripheral nerves.** *Proc Natl Acad Sci U S A*
827 110:16217-22.10.1073/pnas.1303646110

828 Fielder GC, Yang TW, Razdan M, Li Y, Lu J, Perry JK, Lobie PE, and Liu DX (2018). **The**
829 **GDNF Family: A Role in Cancer?** *Neoplasia* 20:99-117.10.1016/j.neo.2017.10.010

Forese MG, Pellegatta M, Canevazzi P, Gullotta GS, Podini P, Rivellini C, Previtali SC, Bacigaluppi M, Quattrini A, and Taveggia C (2020). **Prostaglandin D2 synthase modulates macrophage activity and accumulation in injured peripheral nerves.** *Glia* 68:95-110.10.1002/glia.23705

Ghosh A, Carnahan J, and Greenberg ME (1994). **Requirement for BDNF in activity-dependent survival of cortical neurons.** *Science* 263:1618-1623.10.1126/science.7907431

Goebbels S, Oltrogge JH, Kemper R, Heilmann I, Bormuth I, Wolfer S, Wichert SP, Mobius W, Liu X, Lappe-Siefke C, Rossner MJ, Groszer M, Suter U, Frahm J, Boretius S, and Nave KA (2010). **Elevated phosphatidylinositol 3,4,5-trisphosphate in glia triggers cell-autonomous membrane wrapping and myelination.** *J Neurosci* 30:8953-64.10.1523/JNEUROSCI.0219-10.2010

Gonzalez D, Contreras O, Rebolledo DL, Espinoza JP, van Zundert B, and Brandan E (2017). **ALS skeletal muscle shows enhanced TGF-beta signaling, fibrosis and induction of fibro/adipogenic progenitor markers.** *PLoS One* 12:e0177649.10.1371/journal.pone.0177649

Grinsell D, and Keating CP (2014). **Peripheral nerve reconstruction after injury: a review of clinical and experimental therapies.** *Biomed Res Int* 2014:698256.10.1155/2014/698256

Hammarberg H, Piehl F, Cullheim S, Fjell J, Hokfelt T, and Fried K (1996). **GDNF mRNA in Schwann cells and DRG satellite cells after chronic sciatic nerve injury.** *NeuroReport* 7:857-860.10.1097/00001756-199603220-00004

Han H, Cho JW, Lee S, Yun A, Kim H, Bae D, Yang S, Kim CY, Lee M, Kim E, Lee S, Kang B, Jeong D, Kim Y, Jeon HN, Jung H, Nam S, Chung M, Kim JH, and Lee I (2018). **TRRUST v2: an expanded reference database of human and mouse transcriptional regulatory interactions.** *Nucleic Acids Res* 46:D380-D386.10.1093/nar/gkx1013

Hann SH, Kim SY, Kim YL, Jo YW, Kang JS, Park H, Choi SY, and Kong YY (2024). **Depletion of SMN protein in mesenchymal progenitors impairs the development of bone and neuromuscular junction in spinal muscular atrophy.** *Elife* 12:10.7554/eLife.92731

Hanz S, Perlson E, Willis D, Zheng JQ, Massarwa R, Huerta JJ, Koltzenburg M, Kohler M, van-Minnen J, Twiss JL, and Fainzilber M (2003). **Axoplasmic importins enable retrograde injury signaling in lesioned nerve.** *Neuron* 40:1095-1104.10.1016/s0896-6273(03)00770-0

Hao Y, Hao S, Andersen-Nissen E, Mauck WM, 3rd, Zheng S, Butler A, Lee MJ, Wilk AJ, Darby C, Zager M, Hoffman P, Stoeckius M, Papalexi E, Mimitou EP, Jain J, Srivastava A, Stuart T, Fleming LM, Yeung B, Rogers AJ, McElrath JM, Blish CA, Gottardo R, Smibert P, and Satija R (2021). **Integrated analysis of multimodal single-cell data.** *Cell* 184:3573-3587 e29.10.1016/j.cell.2021.04.048

Heredia JE, Mukundan L, Chen FM, Mueller AA, Deo RC, Locksley RM, Rando TA, and Chawla A (2013). **Type 2 innate signals stimulate fibro/adipogenic progenitors to facilitate muscle regeneration.** *Cell* 153:376-88.10.1016/j.cell.2013.02.053

Hoke A, Gordon T, Zochodne DW, and Sulaiman OA (2002). **A decline in glial cell-line-derived neurotrophic factor expression is associated with impaired regeneration after long-term Schwann cell denervation.** *Exp Neurol* 173:77-85.10.1006/exnr.2001.7826

Jing S, Wen D, Yu Y, Holst PL, Luo Y, Fang M, Tamir R, Antonio L, Hu Z, and Cupples R (1996). **GDNF–induced activation of the ret protein tyrosine kinase is mediated by GDNFR-α, a novel receptor for GDNF.** *Cell* 85:1113-1124.

Joe AW, Yi L, Natarajan A, Le Grand F, So L, Wang J, Rudnicki MA, and Rossi FM (2010). **Muscle injury activates resident fibro/adipogenic progenitors that facilitate myogenesis.** *Nat Cell Biol* 12:153-63.10.1038/ncb2015

Joe AW, Yi L, Natarajan A, Le Grand F, So L, Wang J, Rudnicki MA, and Rossi FM (2010). **Muscle injury activates resident fibro/adipogenic progenitors that facilitate myogenesis.** *Nature cell biology* 12:153-163.

Joseph NM, Mukouyama YS, Mosher JT, Jaegle M, Crone SA, Dormand EL, Lee KF, Meijer D, Anderson DJ, and Morrison SJ (2004). **Neural crest stem cells undergo multilineage differentiation in developing peripheral nerves to generate endoneurial fibroblasts in addition to Schwann cells.** *Development* 131:5599-612.10.1242/dev.01429

Julier Z, Park AJ, Briquez PS, and Martino MM (2017). **Promoting tissue regeneration by modulating the immune system.** *Acta Biomater* 53:13-28.10.1016/j.actbio.2017.01.056

Kalinski AL, Yoon C, Huffman LD, Duncker PC, Kohen R, Passino R, Hafner H, Johnson C, Kawaguchi R, Carbajal KS, Jara JS, Hollis E, Geschwind DH, Segal BM, and Giger RJ (2020). **Analysis of the immune response to sciatic nerve injury identifies efferocytosis as a key mechanism of nerve debridement.** *Elife* 9:10.7554/eLife.60223

Kanehisa M, Furumichi M, Sato Y, Kawashima M, and Ishiguro-Watanabe M (2023). **KEGG for taxonomy-based analysis of pathways and genomes.** *Nucleic Acids Res* 51:D587-D592.10.1093/nar/gkac963

Kim JH, Kang JS, Yoo K, Jeong J, Park I, Park JH, Rhee J, Jeon S, Jo YW, Hann SH, Seo M, Moon S, Um SJ, Seong RH, and Kong YY (2022). **Bap1/SMN axis in Dpp4+ skeletal muscle mesenchymal cells regulates the neuromuscular system.** *JCI Insight* 7:10.1172/jci.insight.158380

Kolberg L, Raudvere U, Kuzmin I, Adler P, Vilo J, and Peterson H (2023). **g:Profiler-interoperable web service for functional enrichment analysis and gene identifier mapping**

(2023 update). *Nucleic Acids Res* 51:W207-W212.10.1093/nar/gkad347

Kucera M, Isserlin R, Arkhangorodsky A, and Bader GD (2016). **AutoAnnotate: A Cytoscape app for summarizing networks with semantic annotations.** *F1000Res* 5:1717.10.12688/f1000research.9090.1

La Manno G, Soldatov R, Zeisel A, Braun E, Hochgerner H, Petukhov V, Lidschreiber K, Kastriti ME, Lonnerberg P, Furlan A, Fan J, Borm LE, Liu Z, van Bruggen D, Guo J, He X, Barker R, Sundstrom E, Castelo-Branco G, Cramer P, Adameyko I, Linnarsson S, and Kharchenko PV (2018). **RNA velocity of single cells.** *Nature* 560:494-498.10.1038/s41586-018-0414-6

Leinroth AP, Mirando AJ, Rouse D, Kobayahsi Y, Tata PR, Rueckert HE, Liao Y, Long JT, Chakkalakal JV, and Hilton MJ (2022). **Identification of distinct non-myogenic skeletal-muscle-resident mesenchymal cell populations.** *Cell Rep* 39:110785.10.1016/j.celrep.2022.110785

Lemos DR, Babaeijandaghi F, Low M, Chang CK, Lee ST, Fiore D, Zhang RH, Natarajan A, Nedospasov SA, and Rossi FM (2015). **Nilotinib reduces muscle fibrosis in chronic muscle injury by promoting TNF-mediated apoptosis of fibro/adipogenic progenitors.** *Nat Med* 21:786-94.10.1038/nm.3869

Lieberman B, Kusi M, Hung CN, Chou CW, He N, Ho YY, Taverna JA, Huang THM, and Chen CL (2021). **Toward uncharted territory of cellular heterogeneity: advances and applications of single-cell RNA-seq.** *J Transl Genet Genom* 5:1-21.10.20517/jtgg.2020.51

Lin H, Ma X, Sun Y, Peng H, Wang Y, Thomas SS, and Hu Z (2022). **Decoding the transcriptome of denervated muscle at single-nucleus resolution.** *J Cachexia Sarcopenia Muscle* 13:2102-2117.10.1002/jcsm.13023

Liu L, Cheung TH, Charville GW, and Rando TA (2015). **Isolation of skeletal muscle stem cells by fluorescence-activated cell sorting.** *Nat Protoc* 10:1612-24.10.1038/nprot.2015.110

Logan M, Martin JF, Nagy A, Lobe C, Olson EN, and Tabin CJ (2002). **Expression of Cre Recombinase in the developing mouse limb bud driven by a Prxl enhancer.** *Genesis* 33:77-80.10.1002/gene.10092

Lukjanenko L, Karaz S, Stuelsatz P, Gurriaran-Rodriguez U, Michaud J, Dammone G, Sizzano F, Mashinchian O, Ancel S, Migliavacca E, Liot S, Jacot G, Metairon S, Raymond F, Descombes P, Palini A, Chazaud B, Rudnicki MA, Bentzinger CF, and Feige JN (2019). **Aging Disrupts Muscle Stem Cell Function by Impairing Matricellular WISP1 Secretion from Fibro-Adipogenic Progenitors.** *Cell Stem Cell* 24:433-446 e7.10.1016/j.stem.2018.12.014

Madaro L, Passafaro M, Sala D, Etxaniz U, Lugarini F, Proietti D, Alfonsi MV, Nicoletti C,

933 Gatto S, De Bardi M, Rojas-Garcia R, Giordani L, Marinelli S, Pagliarini V, Sette C, Sacco A,
934 and Puri PL (2018). **Denervation-activated STAT3-IL-6 signalling in fibro-adipogenic**
935 **progenitors promotes myofibres atrophy and fibrosis.** *Nat Cell Biol* 20:917-
936 927.10.1038/s41556-018-0151-y

937 Magill CK, Tong A, Kawamura D, Hayashi A, Hunter DA, Parsadanian A, Mackinnon SE, and
938 Myckatyn TM (2007). **Reinnervation of the tibialis anterior following sciatic nerve crush**
939 **injury: a confocal microscopic study in transgenic mice.** *Exp Neurol* 207:64-
940 74.10.1016/j.expneurol.2007.05.028

941 Maita KC, Garcia JP, Avila FR, Torres-Guzman RA, Ho O, Chini CCS, Chini EN, and Forte
942 AJ (2023). **Evaluation of the Aging Effect on Peripheral Nerve Regeneration: A**
943 **Systematic Review.** *J Surg Res* 288:329-340.10.1016/j.jss.2023.03.017

944 Malecova B, Gatto S, Etxaniz U, Passafaro M, Cortez A, Nicoletti C, Giordani L, Torcinaro A,
945 De Bardi M, Bicciato S, De Santa F, Madaro L, and Puri PL (2018). **Dynamics of cellular**
946 **states of fibro-adipogenic progenitors during myogenesis and muscular dystrophy.** *Nat*
947 *Commun* 9:3670.10.1038/s41467-018-06068-6

948 Mallik A, and Weir AI (2005). **Nerve conduction studies: essentials and pitfalls in practice.**
949 *J Neurol Neurosurg Psychiatry* 76 Suppl 2:ii23-31.10.1136/jnnp.2005.069138

950 Merico D, Isserlin R, Stueker O, Emili A, and Bader GD (2010). **Enrichment map: a**
951 **network-based method for gene-set enrichment visualization and interpretation.** *PLoS*
952 *One* 5:e13984.10.1371/journal.pone.0013984

953 Mueller M, Wacker K, Ringelstein EB, Hickey WF, Imai Y, and Kiefer R (2001). **Rapid**
954 **response of identified resident endoneurial macrophages to nerve injury.** *Am J Pathol*
955 159:2187-97.10.1016/S0002-9440(10)63070-2

956 Murphy MM, Lawson JA, Mathew SJ, Hutcheson DA, and Kardon G (2011). **Satellite cells,**
957 **connective tissue fibroblasts and their interactions are crucial for muscle regeneration.**
958 *Development* 138:3625-37.10.1242/dev.064162

959 Nicoletti C, Wei X, Etxaniz U, D'Ercole C, Madaro L, Perera R, and Puri PL (2023). **Muscle**
960 **denervation promotes functional interactions between glial and mesenchymal cells**
961 **through NGFR and NGF.** *iScience* 26:107114.10.1016/j.isci.2023.107114

962 Nicoletti C, Wei X, Etxaniz U, Proietti D, Madaro L, and Puri PL (2020). **scRNA-seq-based**
963 **analysis of skeletal muscle response to denervation reveals selective activation of muscle-**
964 **resident glial cells and fibroblasts.** *Biorxiv* 10.1101/2020.12.29.424762

965 Oprescu SN, Yue F, Qiu J, Brito LF, and Kuang S (2020). **Temporal Dynamics and**
966 **Heterogeneity of Cell Populations during Skeletal Muscle Regeneration.** *iScience*

967 23:100993.10.1016/j.isci.2020.100993

968 Ortega-Gomez A, Perretti M, and Soehnlein O (2013). **Resolution of inflammation: an**
969 **integrated view.** *EMBO Mol Med* 5:661-74.10.1002/emmm.201202382

970 Oudega M, and Hagg T (1999). **Neurotrophins promote regeneration of sensory axons in**
971 **the adult rat spinal cord.** *Brain Research* 818:431-438.

972 Painter MW, Brosius Lutz A, Cheng YC, Latremoliere A, Duong K, Miller CM, Posada S,
973 Cobos EJ, Zhang AX, Wagers AJ, Havton LA, Barres B, Omura T, and Woolf CJ (2014).
974 **Diminished Schwann cell repair responses underlie age-associated impaired axonal**
975 **regeneration.** *Neuron* 83:331-343.10.1016/j.neuron.2014.06.016

976 Parrinello S, Napoli I, Ribeiro S, Wingfield Digby P, Fedorova M, Parkinson DB, Doddrell RD,
977 Nakayama M, Adams RH, and Lloyd AC (2010). **EphB signaling directs peripheral nerve**
978 **regeneration through Sox2-dependent Schwann cell sorting.** *Cell* 143:145-
979 55.10.1016/j.cell.2010.08.039

980 Proietti D, Giordani L, De Bardi M, D'Ercole C, Lozanoska-Ochser B, Amadio S, Volonte C,
981 Marinelli S, Muchir A, Bouche M, Borsellino G, Sacco A, Puri PL, and Madaro L (2021).
982 **Activation of skeletal muscle-resident glial cells upon nerve injury.** *JCI Insight*
983 6:10.1172/jci.insight.143469

984 Reimand J, Isserlin R, Voisin V, Kucera M, Tannus-Lopes C, Rostamianfar A, Wadi L, Meyer
985 M, Wong J, Xu C, Merico D, and Bader GD (2019). **Pathway enrichment analysis and**
986 **visualization of omics data using g:Profiler, GSEA, Cytoscape and EnrichmentMap.** *Nat*
987 *Protoc* 14:482-517.10.1038/s41596-018-0103-9

988 Roberts EW, Deonarine A, Jones JO, Denton AE, Feig C, Lyons SK, Espeli M, Kraman M,
989 McKenna B, Wells RJ, Zhao Q, Caballero OL, Larder R, Coll AP, O'Rahilly S, Brindle KM,
990 Teichmann SA, Tuveson DA, and Fearon DT (2013). **Depletion of stromal cells expressing**
991 **fibroblast activation protein-alpha from skeletal muscle and bone marrow results in**
992 **cachexia and anemia.** *J Exp Med* 210:1137-51.10.1084/jem.20122344

993 Saito Y, Chikenji TS, Matsumura T, Nakano M, and Fujimiya M (2020). **Exercise enhances**
994 **skeletal muscle regeneration by promoting senescence in fibro-adipogenic progenitors.**
995 *Nat Commun* 11:889.10.1038/s41467-020-14734-x

996 Sariola H, and Saarma M (2003). **Novel functions and signalling pathways for GDNF.** *J Cell*
997 *Sci* 116:3855-62.10.1242/jcs.00786

998 Scheib J, and Hoke A (2013). **Advances in peripheral nerve regeneration.** *Nat Rev Neurol*
999 9:668-76.10.1038/nrneurol.2013.227

1000 Scheib JL, and Hoke A (2016). **An attenuated immune response by Schwann cells and**
1001 **macrophages inhibits nerve regeneration in aged rats.** *Neurobiol Aging* 45:1-
1002 9.10.1016/j.neurobiolaging.2016.05.004

1003 Scott RW, Arostegui M, Schweitzer R, Rossi FMV, and Underhill TM (2019). **Hic1 Defines**
1004 **Quiescent Mesenchymal Progenitor Subpopulations with Distinct Functions and Fates in**
1005 **Skeletal Muscle Regeneration.** *Cell Stem Cell* 25:797-813 e9.10.1016/j.stem.2019.11.004

1006 Shannon P, Markiel A, Ozier O, Baliga NS, Wang JT, Ramage D, Amin N, Schwikowski B,
1007 and Ideker T (2003). **Cytoscape: a software environment for integrated models of**
1008 **biomolecular interaction networks.** *Genome Res* 13:2498-504.10.1101/gr.1239303

1009 Takemura Y, Imai S, Kojima H, Katagi M, Yamakawa I, Kasahara T, Urabe H, Terashima T,
1010 Yasuda H, Chan L, Kimura H, and Matsusue Y (2012). **Brain-derived neurotrophic factor**
1011 **from bone marrow-derived cells promotes post-injury repair of peripheral nerve.** *PLoS*
1012 *One* 7:e44592.10.1371/journal.pone.0044592

1013 Theret M, Rossi FMV, and Contreras O (2021). **Evolving Roles of Muscle-Resident Fibro-**
1014 **Adipogenic Progenitors in Health, Regeneration, Neuromuscular Disorders, and Aging.**
1015 *Front Physiol* 12:673404.10.3389/fphys.2021.673404

1016 Toma JS, Karamboulas K, Carr MJ, Kolaj A, Yuzwa SA, Mahmud N, Storer MA, Kaplan DR,
1017 and Miller FD (2020). **Peripheral Nerve Single-Cell Analysis Identifies Mesenchymal**
1018 **Ligands that Promote Axonal Growth.** *eNeuro* 7:10.1523/ENEURO.0066-20.2020

1019 Treanor JJ, Goodman L, de Sauvage F, Stone DM, Poulsen KT, Beck CD, Gray C, Armanini
1020 MP, Pollock RA, and Hefti F (1996). **Characterization of a multicomponent receptor for**
1021 **GDNF.** *Nature* 382:80-83.

1022 Trupp M, Arenas E, Fainzilber M, Nilsson AS, Sieber BA, Grigoriou M, Kilkenny C, Salazar-
1023 Grueso E, Pachnis V, Arumae U, Sariola H, Saarma M, and Ibanez CF (1996). **Functional**
1024 **receptor for GDNF encoded by the c-ret proto-oncogene.** *Nature* 381:785-
1025 789.10.1038/381785a0

1026 Uezumi A, Fukada S-i, Yamamoto N, Takeda Si, and Tsuchida K (2010). **Mesenchymal**
1027 **progenitors distinct from satellite cells contribute to ectopic fat cell formation in skeletal**
1028 **muscle.** *Nature cell biology* 12:143-152.

1029 Uezumi A, Fukada S, Yamamoto N, Takeda S, and Tsuchida K (2010). **Mesenchymal**
1030 **progenitors distinct from satellite cells contribute to ectopic fat cell formation in skeletal**
1031 **muscle.** *Nat Cell Biol* 12:143-52.10.1038/ncb2014

1032 Uezumi A, Ikemoto-Uezumi M, and Tsuchida K (2014). **Roles of nonmyogenic mesenchymal**
1033 **progenitors in pathogenesis and regeneration of skeletal muscle.** *Front Physiol*

5:68.10.3389/fphys.2014.00068

Uezumi A, Ikemoto-Uezumi M, Zhou H, Kurosawa T, Yoshimoto Y, Nakatani M, Hitachi K, Yamaguchi H, Wakatsuki S, Araki T, Morita M, Yamada H, Toyoda M, Kanazawa N, Nakazawa T, Hino J, Fukada SI, and Tsuchida K (2021). **Mesenchymal Bmp3b expression maintains skeletal muscle integrity and decreases in age-related sarcopenia.** *J Clin Invest* 131:10.1172/JCI139617

Uezumi A, Ito T, Morikawa D, Shimizu N, Yoneda T, Segawa M, Yamaguchi M, Ogawa R, Matev MM, Miyagoe-Suzuki Y, Takeda S, Tsujikawa K, Tsuchida K, Yamamoto H, and Fukada S (2011). **Fibrosis and adipogenesis originate from a common mesenchymal progenitor in skeletal muscle.** *J Cell Sci* 124:3654-64.10.1242/jcs.086629

Vallecillo-Garcia P, Orgeur M, Vom Hofe-Schneider S, Stumm J, Kappert V, Ibrahim DM, Borno ST, Hayashi S, Relaix F, Hildebrandt K, Sengle G, Koch M, Timmermann B, Marazzi G, Sassoon DA, Duprez D, and Stricker S (2017). **Odd skipped-related 1 identifies a population of embryonic fibro-adipogenic progenitors regulating myogenesis during limb development.** *Nat Commun* 8:1218.10.1038/s41467-017-01120-3

Verdú E, Ceballos D, Vilches JJ, and Navarro X (2008). **Influence of aging on peripheral nerve function and regeneration.** *Journal of the Peripheral Nervous System* 5:191-208.10.1111/j.1529-8027.2000.00026.x

Wagstaff LJ, Gomez-Sanchez JA, Fazal SV, Otto GW, Kilpatrick AM, Michael K, Wong LYN, Ma KH, Turmaine M, Svaren J, Gordon T, Arthur-Farraj P, Velasco-Aviles S, Cabedo H, Benito C, Mirsky R, and Jessen KR (2021). **Failures of nerve regeneration caused by aging or chronic denervation are rescued by restoring Schwann cell c-Jun.** *Elife* 10:10.7554/eLife.62232

Wilhelm JC, Xu M, Cucoranu D, Chmielewski S, Holmes T, Lau KS, Bassell GJ, and English AW (2012). **Cooperative roles of BDNF expression in neurons and Schwann cells are modulated by exercise to facilitate nerve regeneration.** *J Neurosci* 32:5002-9.10.1523/JNEUROSCI.1411-11.2012

Wosczyna MN, Konishi CT, Perez Carbajal EE, Wang TT, Walsh RA, Gan Q, Wagner MW, and Rando TA (2019). **Mesenchymal Stromal Cells Are Required for Regeneration and Homeostatic Maintenance of Skeletal Muscle.** *Cell Rep* 27:2029-2035 e5.10.1016/j.celrep.2019.04.074

Xiao J, Wong AW, Willingham MM, Kaasinen SK, Hendry IA, Howitt J, Putz U, Barrett GL, Kilpatrick TJ, and Murray SS (2009). **BDNF exerts contrasting effects on peripheral myelination of NGF-dependent and BDNF-dependent DRG neurons.** *J Neurosci* 29:4016-22.10.1523/JNEUROSCI.3811-08.2009

1069 Xu P, Rosen KM, Hedstrom K, Rey O, Guha S, Hart C, and Corfas G (2013). **Nerve injury**
1070 **induces glial cell line-derived neurotrophic factor (GDNF) expression in Schwann cells**
1071 **through purinergic signaling and the PKC-PKD pathway.** *Glia* 61:1029-
1072 40.10.1002/glia.22491

1073 Zhang JY, Luo XG, Xian CJ, Liu ZH, and Zhou XF (2000). **Endogenous BDNF is required**
1074 **for myelination and regeneration of injured sciatic nerve in rodents.** *European Journal of*
1075 *Neuroscience* 12:4171-4180.10.1111/j.1460-9568.2000.01312.x

1076 Zhao XF, Huffman LD, Hafner H, Athaiya M, Finneran MC, Kalinski AL, Kohen R, Flynn C,
1077 Passino R, Johnson CN, Kohrman D, Kawaguchi R, Yang LJS, Twiss JL, Geschwind DH,
1078 Corfas G, and Giger RJ (2022). **The injured sciatic nerve atlas (iSNAT), insights into the**
1079 **cellular and molecular basis of neural tissue degeneration and regeneration.** *Elife*
1080 11:10.7554/eLife.80881

1081 Zheng J, Sun J, Lu X, Zhao P, Li K, and Li L (2016). **BDNF promotes the axonal regrowth**
1082 **after sciatic nerve crush through intrinsic neuronal capability upregulation and distal**
1083 **portion protection.** *Neurosci Lett* 621:1-8.10.1016/j.neulet.2016.04.006

1084

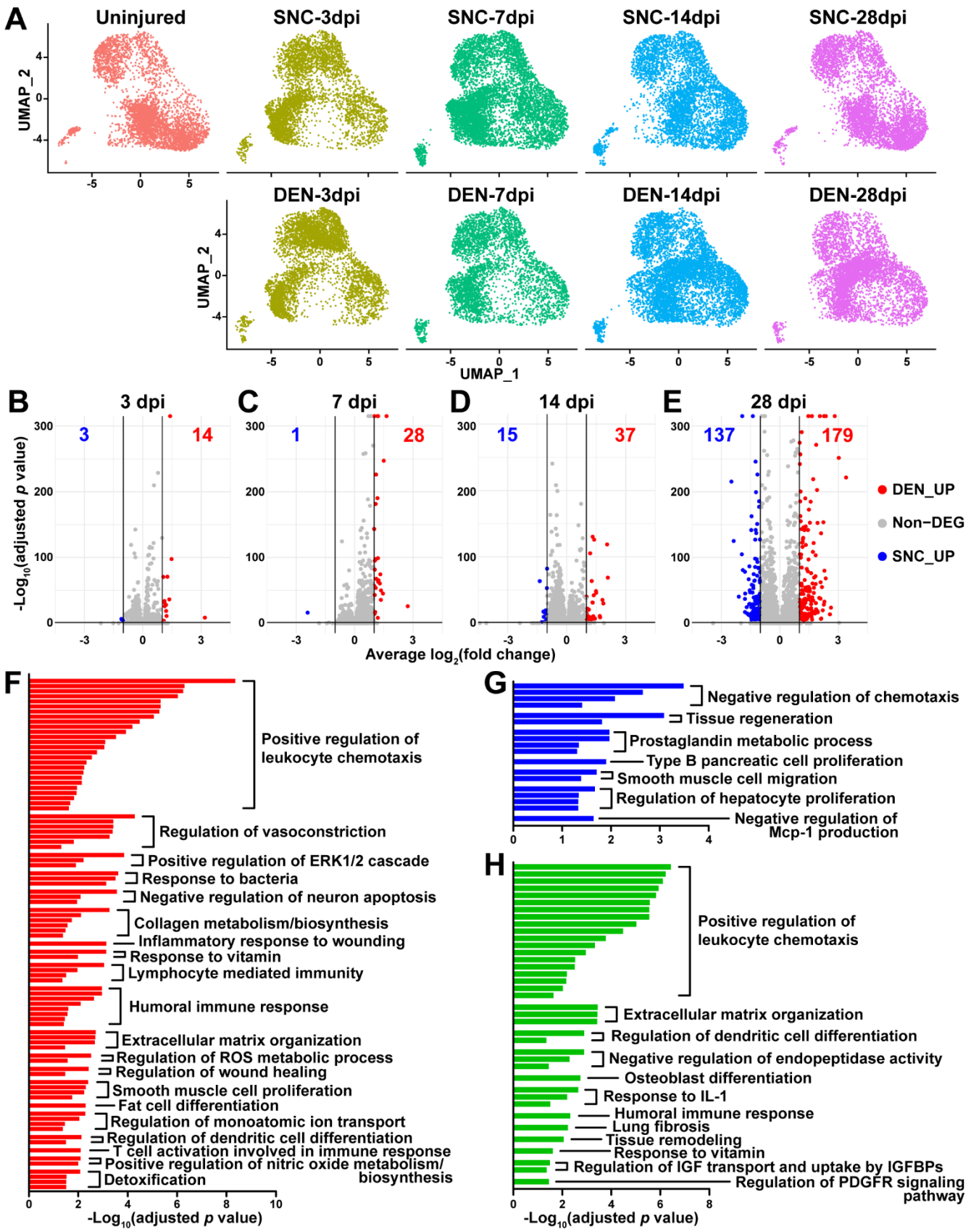

Figure 1. Distinct response profiles of FAPs upon nerve crush injury versus denervation.
(**A**) Single-cell transcriptome data of nerve injury-affected FAPs displayed separately by samples on UMAP plots. See Figure 1—figure supplement 1A for experimental design. (**B**–**E**) Volcano plots showing different numbers of DEGs identified from comparing SNC- vs DEN-affected FAPs at (B) 3, (C) 7, (D) 14, (E) 28 days post injury (dpi). (**F**–**H**) Pathway terms enriched from gene set overrepresentation analyses using g:Profiler. DEGs used as input were (F) DEN-28dpi-upregulated versus SNC-28dpi, (G) SNC-28dpi-upregulated versus DEN-28dpi, and (H) DEGs upregulated commonly in SNC-3dpi, SNC-7dpi, DEN-3dpi, and DEN-7dpi versus uninjured control.

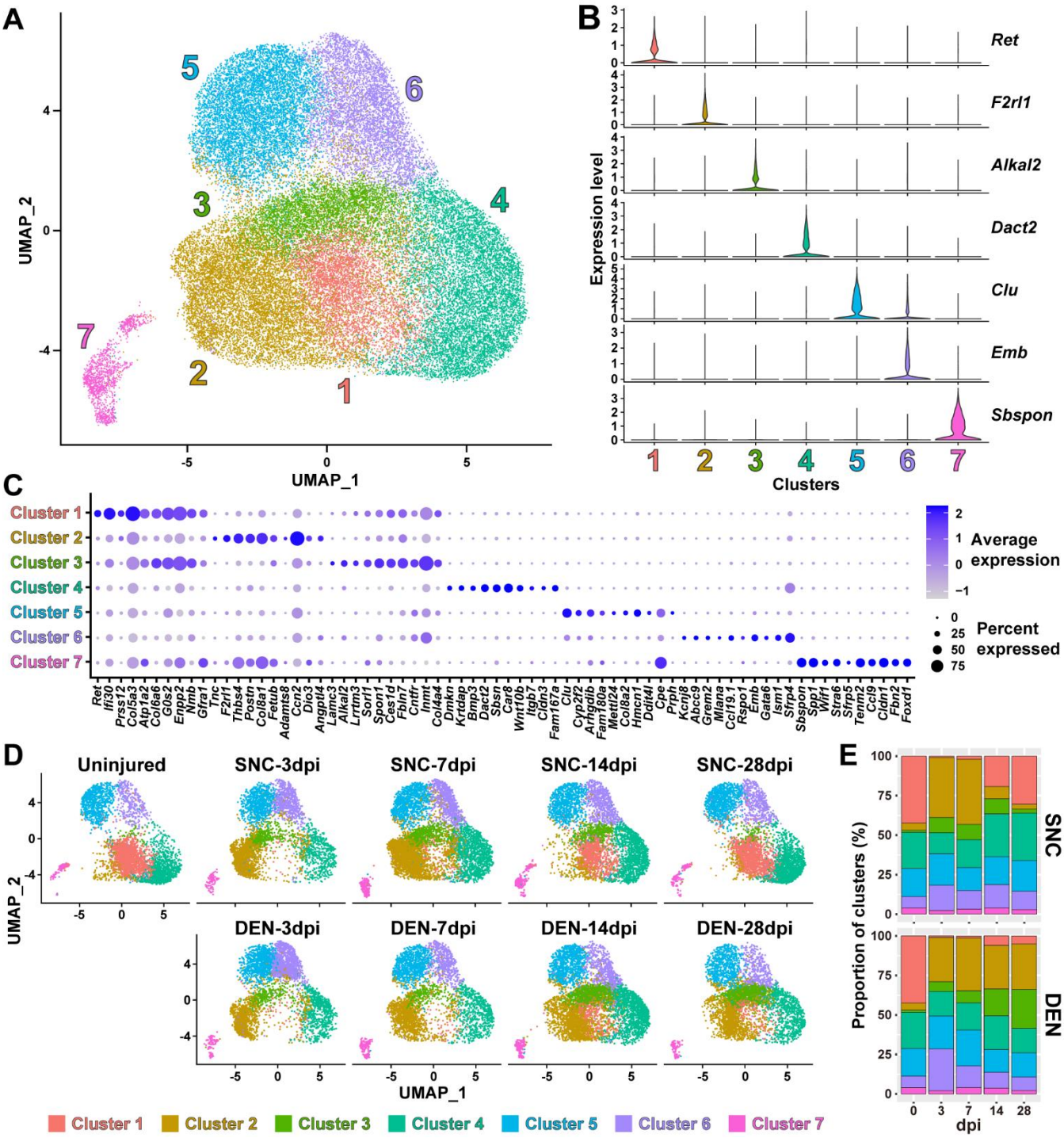

Figure 2. Nerve injury-responsive subsets within FAPs.
(**A**) Seven clusters identified by unsupervised clustering using all nine scRNA-seq samples obtained in this study displayed on the UMAP plot. (**B**) Violin plots showing expressions of unique marker genes identified in each cluster. (**C**) Dotplot showing the expression levels and percentages of top 10 DEGs enriched in each cluster. (**D**) UMAP plots of clustered scRNA-seq data displayed separately by samples. (**E**) Barplots showing the proportions of the seven clusters that comprise each scRNA-seq sample of nerve injury-affected FAPs. For 0 dpi, data from the same uninjured control sample is displayed for both SNC and DEN.

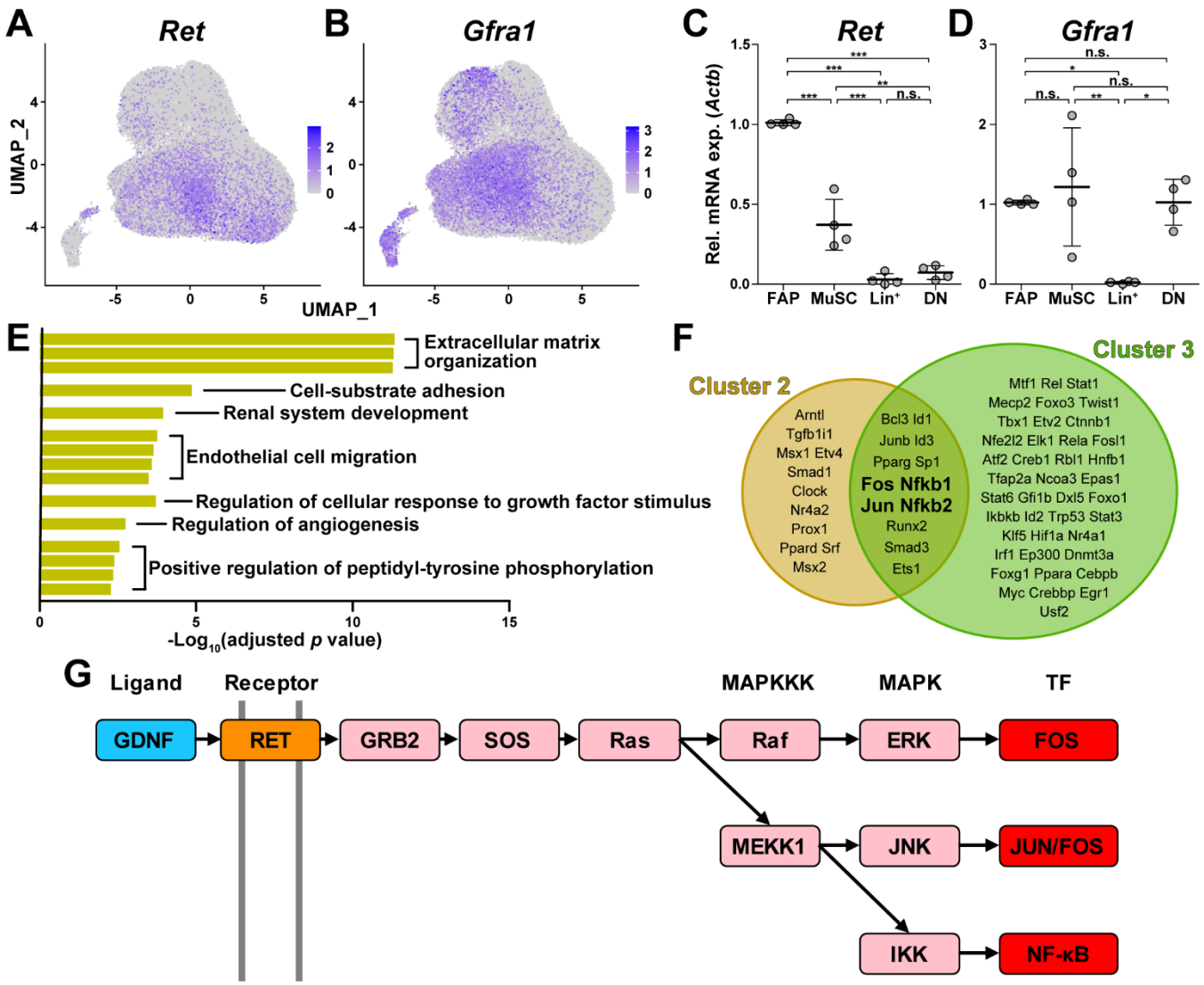

Figure 3. GDNF signaling pathway in the nerve injury-sensing mechanism by FAPs.
(**A**–**B**) UMAP plots showing the expressions of (A) *Ret* and (B) *Gfra1* in the merged scRNA-seq data. (**C**–**D**) RT-qPCR results showing the expressions of (C) *Ret* and (D) *Gfra1* in mononuclear cells isolated from uninjured muscles by FACS. See Figure 1—figure supplement 1B for the FACS isolation scheme. MuSC, muscle stem cells; Lin$^+$, lineage-positive cells; DN, Vcam1/Sca1 double-negative cells. n = 4; one-way ANOVA with Bonferroni's post hoc test. * $p < 0.05$, ** $p < 0.01$, *** $p < 0.001$, n.s., not significant. (**E**) Shared pathway terms commonly identified from gene set overrepresentation analyses using DEGs specifically upregulated in clusters 1, 2 or 3. See Figure 3—figure supplements 1B, 2A, and 2B for the full ORA results. (**F**) Venn diagram showing the results from TRRUST analyses using DEGs enriched in clusters 2 and 3. Transcription factors predicted to regulate genes upregulated in each cluster are listed. (**G**) Simplified diagram of the GDNF/RET-MAPK signaling pathway. Blue: GDNF ligand; orange: GDNF receptor RET expressed in cluster 1; pink: downstream cascade genes expressed in clusters 1-3; red: transcription factors commonly predicted to regulate upregulated genes in clusters 2 and 3.

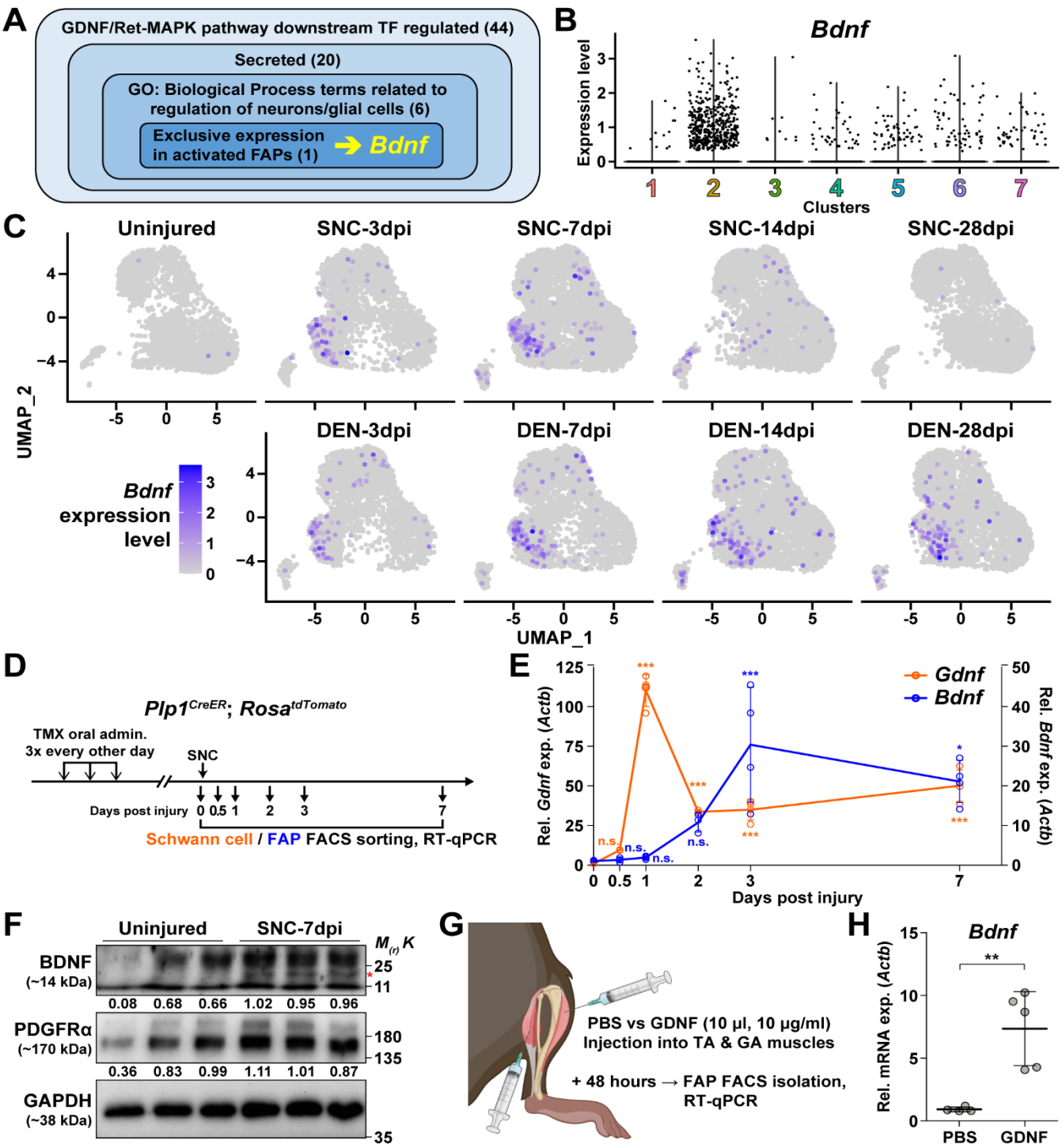

Figure 4. The GDNF-BDNF axis as FAP's response mechanism to nerve injury.
(**A**) Identification of candidate genes expressed in FAPs in response to GDNF that may contribute to nerve regeneration. Number of genes that fit into each criterion is indicated. (**B**) Violin plot displaying the expression levels of *Bdnf* in the seven FAP clusters. (**C**) Expression of *Bdnf* in each scRNA-seq sample shown on UMAP plots. (**D**) Scheme for sampling Schwann cells and FAPs at different time points post SNC for gene expression analyses. (**E**) RT-qPCR results showing expression levels of *Gdnf* in Schwann cells (orange dot and line, left y-axis) and *Bdnf* in FAPs (blue dot and line, right y-axis) at different time points post SNC. n = 4, except for 0 and 2 dpi, where n = 3. One-way ANOVA with Bonferroni's post hoc test. * $p < 0.05$, *** $p < 0.001$, n.s., not significant. (**F**) Western blot results showing BDNF protein expression in PDGFRα$^+$ FAPs isolated from SNC-affected or uninjured contralateral muscles at 7 dpi. n = 3. Mature form of BDNF is indicated with a red asterisk. Quantified values normalized to GAPDH is indicated below each protein. See Figure 4—figure supplement 1 for the experimental scheme. (**G**) Scheme for intramuscular injection of either PBS or recombinant mouse GDNF protein, with the time point for FAP isolation post injection indicated. (**H**) RT-qPCR results showing the expression level of *Bdnf* in FAPs 48 hours post intramuscular injection of either PBS (n = 4) or GDNF (n = 5). Unpaired t-test with Welch's correction. ** $p < 0.01$.

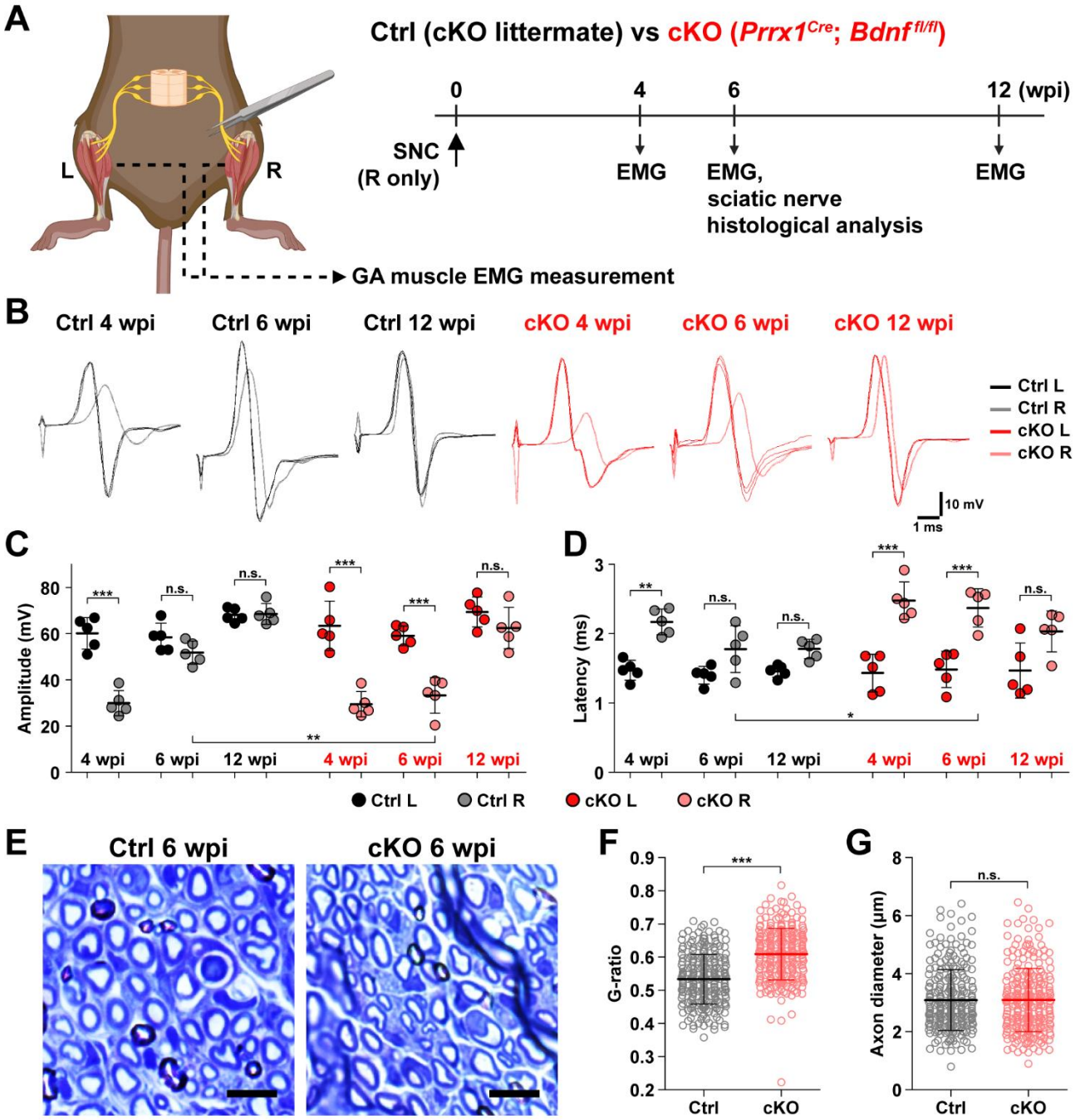

Figure 5. Remyelination by FAP-derived BDNF during peripheral nerve regeneration.
(**A**) Experimental scheme displaying mice used and the time points selected for EMG measurements and sciatic nerve dissection. wpi, weeks post injury. See Figure 5—figure supplement 1D for the EMG measurement scheme. (**B**) Representative EMG measurement results of both injured and uninjured GA muscles from Ctrl or cKO mice at the indicated time points post SNC. (**C**–**D**) Quantified results of EMG measurement showing (C) CMAP amplitude and (D) CMAP latency. n = 5. One-way ANOVA with Bonferroni's post hoc test. * $p < 0.05$, ** $p < 0.01$, *** $p < 0.001$, n.s., not significant. See Figure 5—figure supplement 1E for the EMG measurement quantification metholodogy. (**E**) Representative images showing toluidine blue-stained, semi-thin cross-sections of sciatic nerves dissected from Ctrl or cKO mice at 6 wpi. Scale bars, 10 μm. (**F**–**G**) Quantification of (F) calculated G-ratio values and (G) axon diameters from analyzing toluidine blue-stained sciatic nerve sections dissected from Ctrl or cKO mice at 6 wpi. 50 axons were randomly selected from each sciatic nerve for quantification. n = 5. Mann-Whitney U test. *** $p < 0.001$, n.s., not significant. See Figure 5—figure supplement 1F and G for G-ratio quantification scheme and methodology.

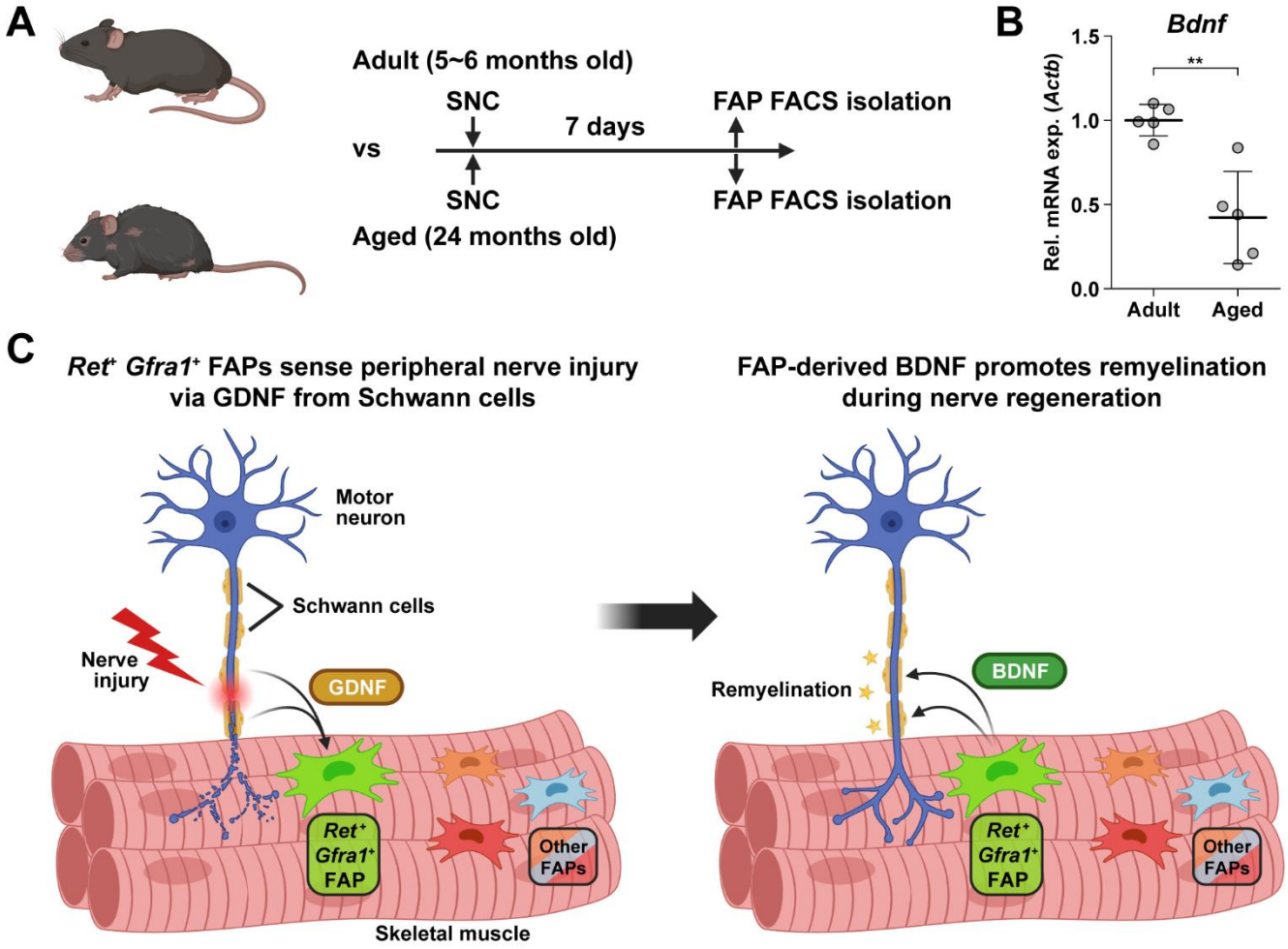

Figure 6. Implication of FAP-derived BDNF in the age-related delay in nerve regeneration.
(**A**) Experimental scheme indicating ages of mice used and the time point for FAP isolation to compare the expression level of *Bdnf* post SNC. (**B**) RT-qPCR results showing the expression level of *Bdnf* in FAPs isolated from either adult (5-6 months) or aged (24 months) mice at 7 dpi. n = 5. Unpaired t-test. ** $p < 0.01$. (**C**) Graphical summary of this study.

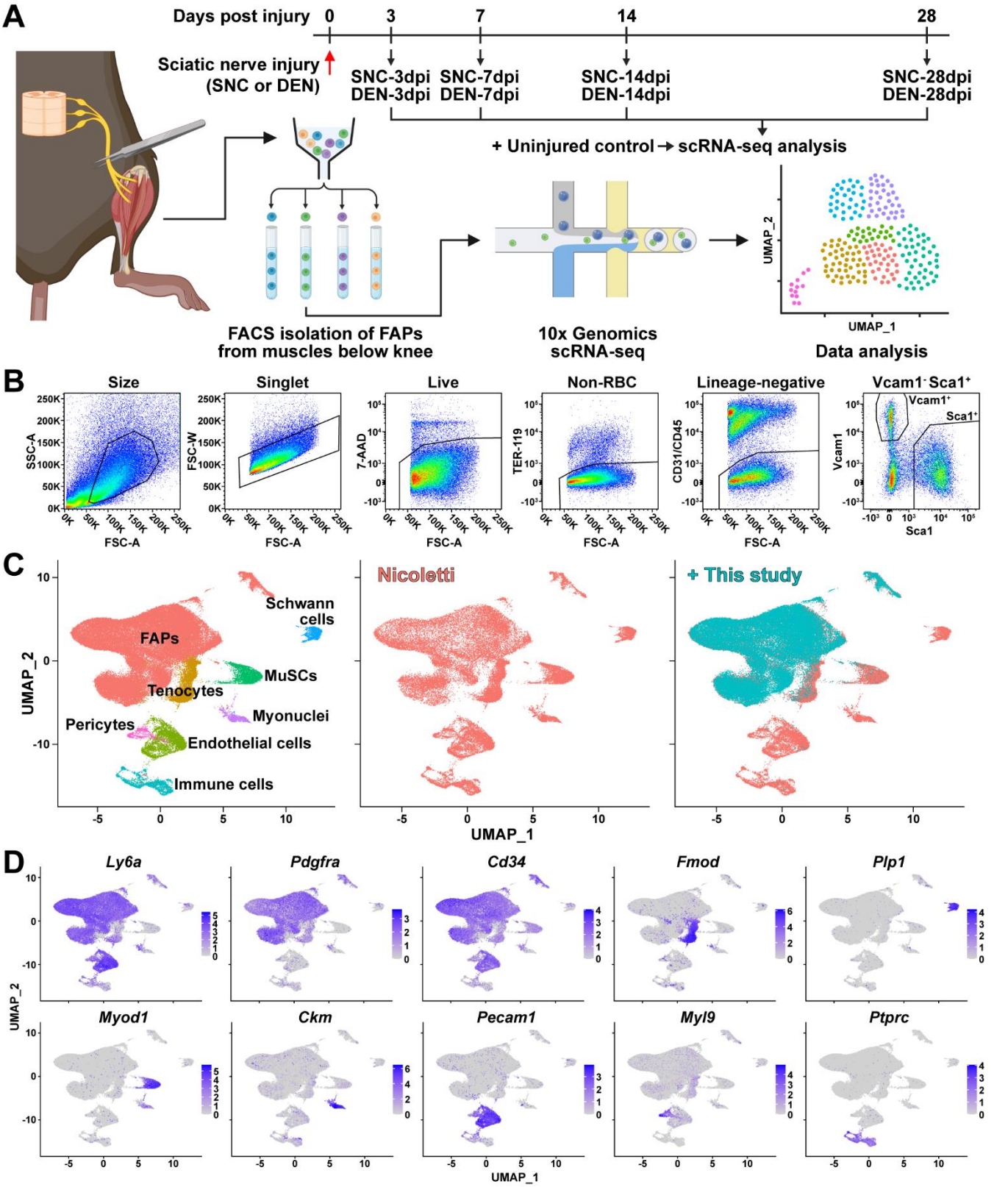

Figure 1—figure supplement 1. Establishment and validation of nerve injury-affected FAPs' scRNA-seq data.

(**A**) Experimental scheme depicting the procedures for sample collection and scRNA-seq. The types of nerve injuries and time points for FAP isolation for each sample are specified. (**B**) Gating strategies used for FACS isolation of FAPs. (**C**) Integration of scRNA-seq data obtained in this study and data from Nicoletti et al. (2023) visualized on UMAP plots. Left: integrated data labeled with cell types; middle: cells from Nicoletti et al. (2023) only; right: data from this study overlaid on top of data from Nicoletti et al. (2023). (**D**) Expressions of marker genes that distinguish cell types within skeletal muscle in the integrated scRNA-seq data visualized on UMAP plots.

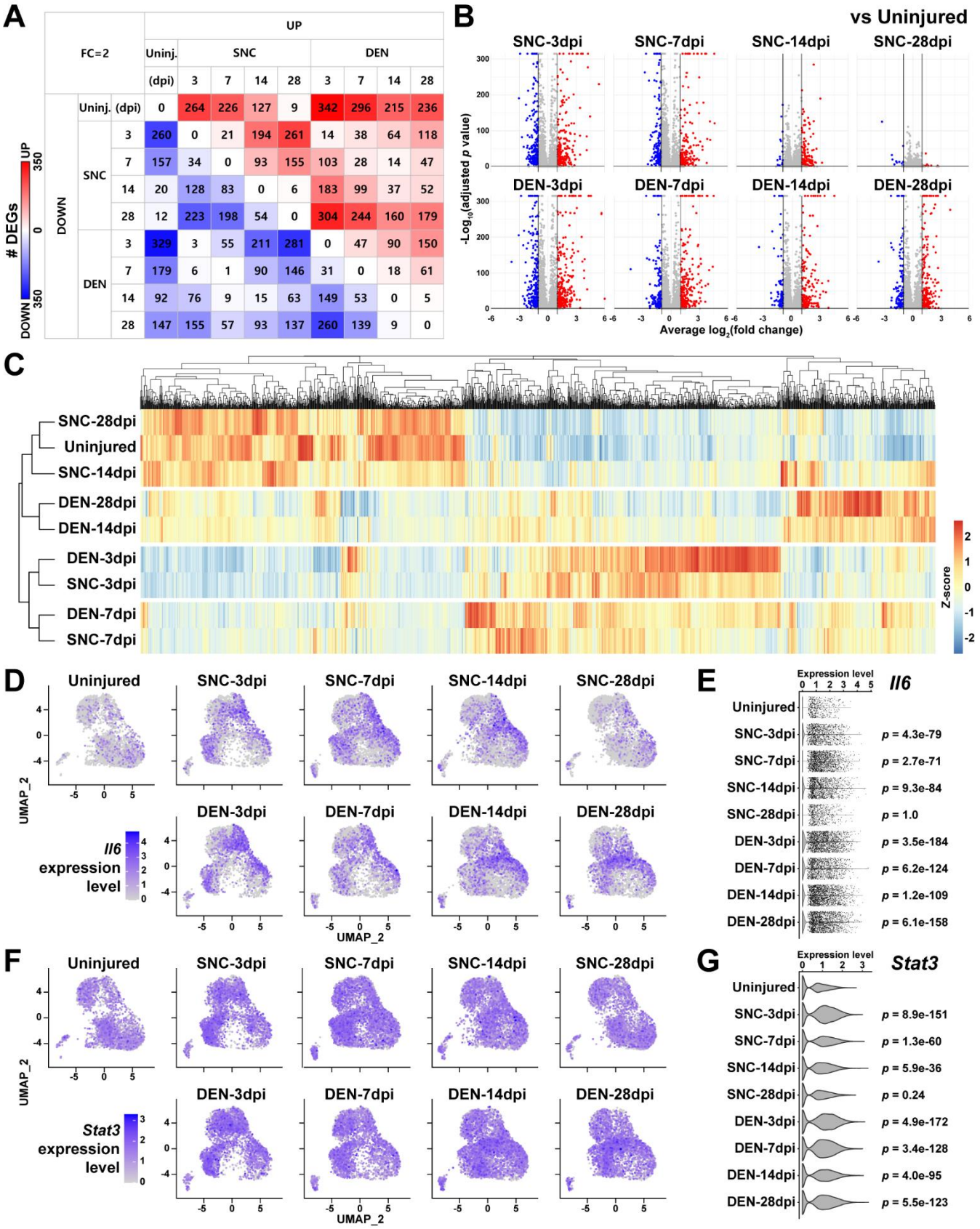

Figure 1—figure supplement 2. DEG analyses reveal similarities and differences between FAPs affected by SNC or DEN at different time points.

(**A**) Number of DEGs identified from pairwise comparisons of all nine scRNA-seq samples visualized as a heatmap. (**B**) DEGs identified from comparing nerve injury-affected FAPs versus uninjured control shown on volcano plots. (**C**) Hierarchical clustering of the nine scRNA-seq samples using DEGs identified in (A) displayed as a heatmap. (**D** and **F**) UMAP plots showing the expressions of (D) *Il6* and (F) *Stat3*. (**E** and **G**) Violin plots showing the expressions of (E) *Il6* and (G) *Stat3*, with *p* values calculated from comparing each sample to uninjured control. Wilcoxon rank sum test.

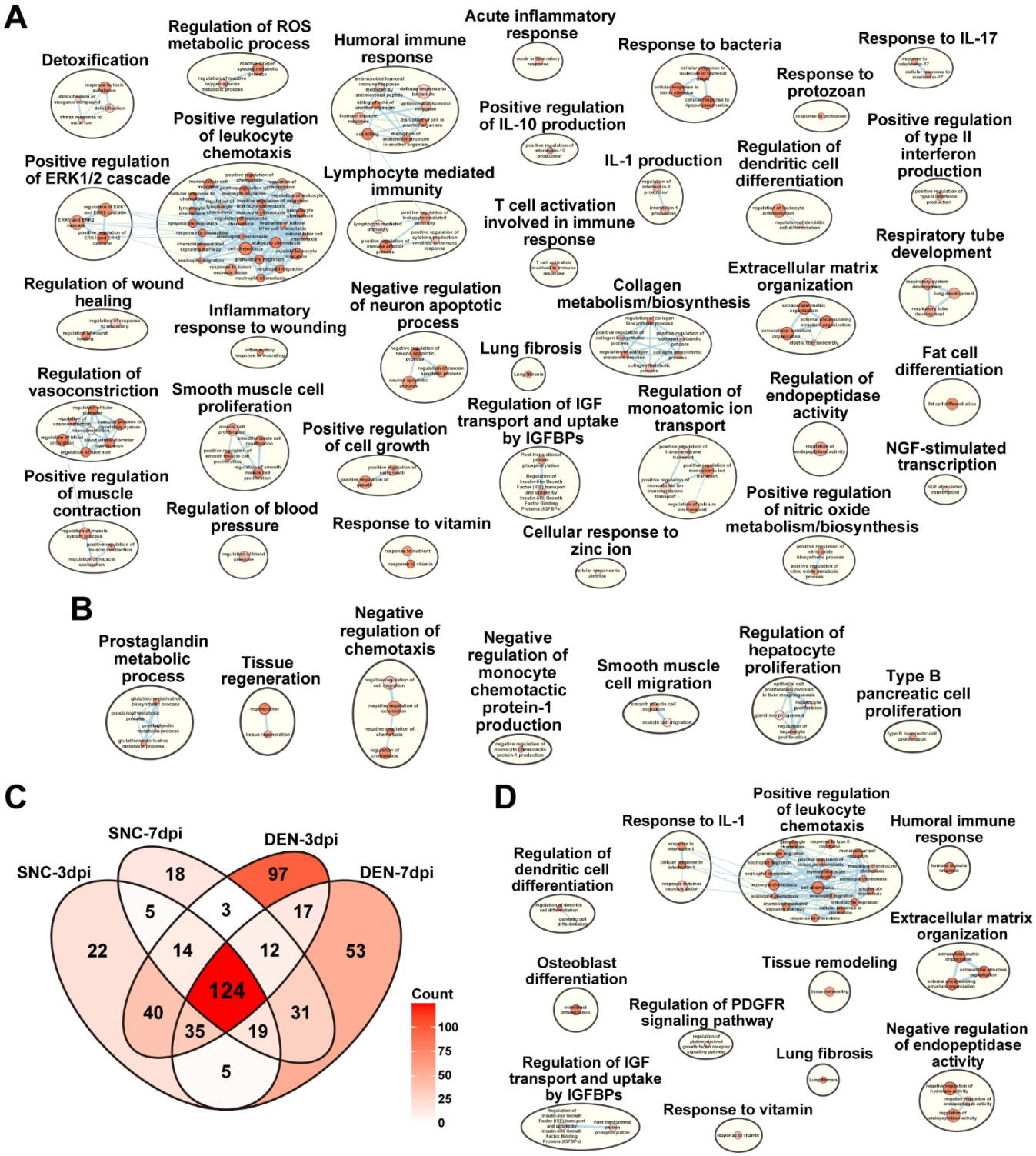

Figure 1—figure supplement 3. Gene set overrepresentation analyses using DEGs from pairwise comparisons of the nine scRNA-seq samples.

(**A**–**B**) Results from g:Profiler showing pathways enriched using DEGs upregulated in (A) DEN-28dpi versus SNC-28dpi and (B) vice versa. (**C**) Venn diagram showing the number of overlapping genes identified as DEGs by comparing each indicated sample to uninjured control. (**D**) Results from g:Profiler showing pathways enriched using DEGs shared in all four samples compared to uninjured control, as shown in (C).

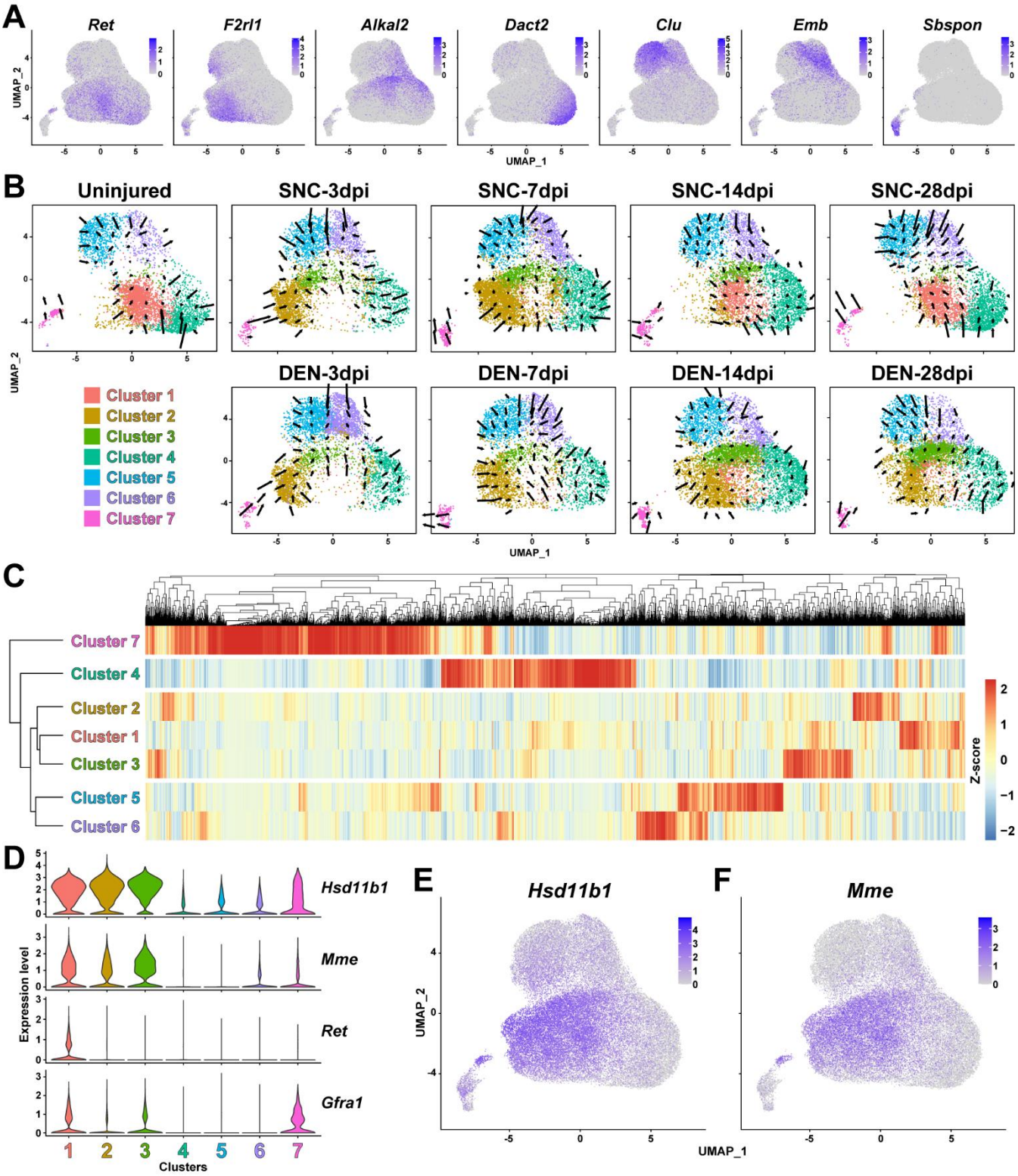

Figure 2—figure supplement 1. Identification of FAP clusters that respond to nerve injury.
(**A**) UMAP plots showing expressions of cluster-specific marker genes identified in this study. (**B**) Results from RNA velocity analysis visualized on UMAP plots. Arrows indicate the predicted direction of cellular movement in the near future on the UMAP plots. (**C**) Hierarchical clustering of the seven FAP clusters displayed with a heatmap. (**D**) Violin plots showing the expressions of marker genes previously reported by Leinroth et al. (2022) in the seven clusters identified in this study. (**E**–**F**) Expressions of (E) *Hsd11b1* and (F) *Mme* shown on UMAP plots.

A

Gene	Average $\log_2$FC	Adjusted *p* value
Ret	2.266	$<10^{-303}$
Ifi30	1.706	
Prss12	1.665	
Col5a3	1.573	
Atp1a2	1.543	
Col6a6	1.455	
G0s2	1.451	
Enpp2	1.427	
Nmb	1.412	
Gfra1	1.395	

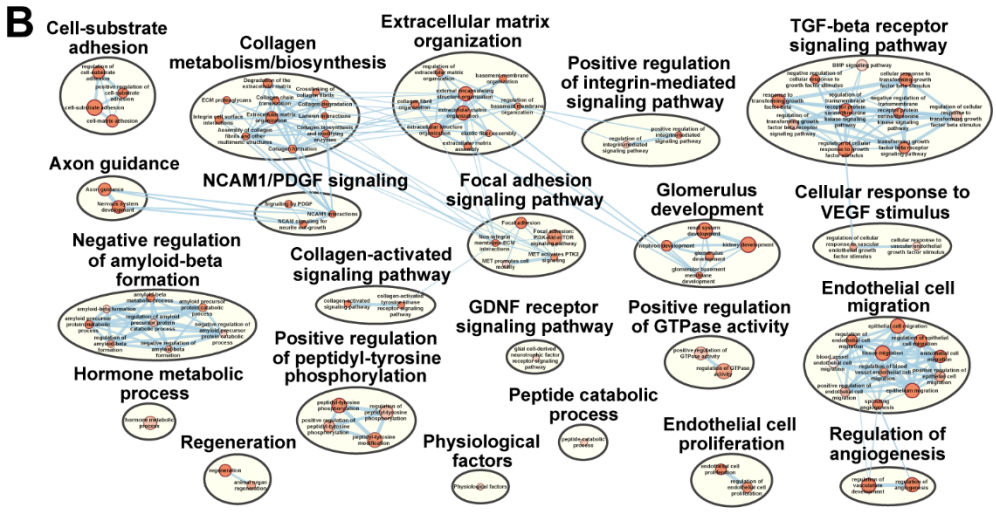

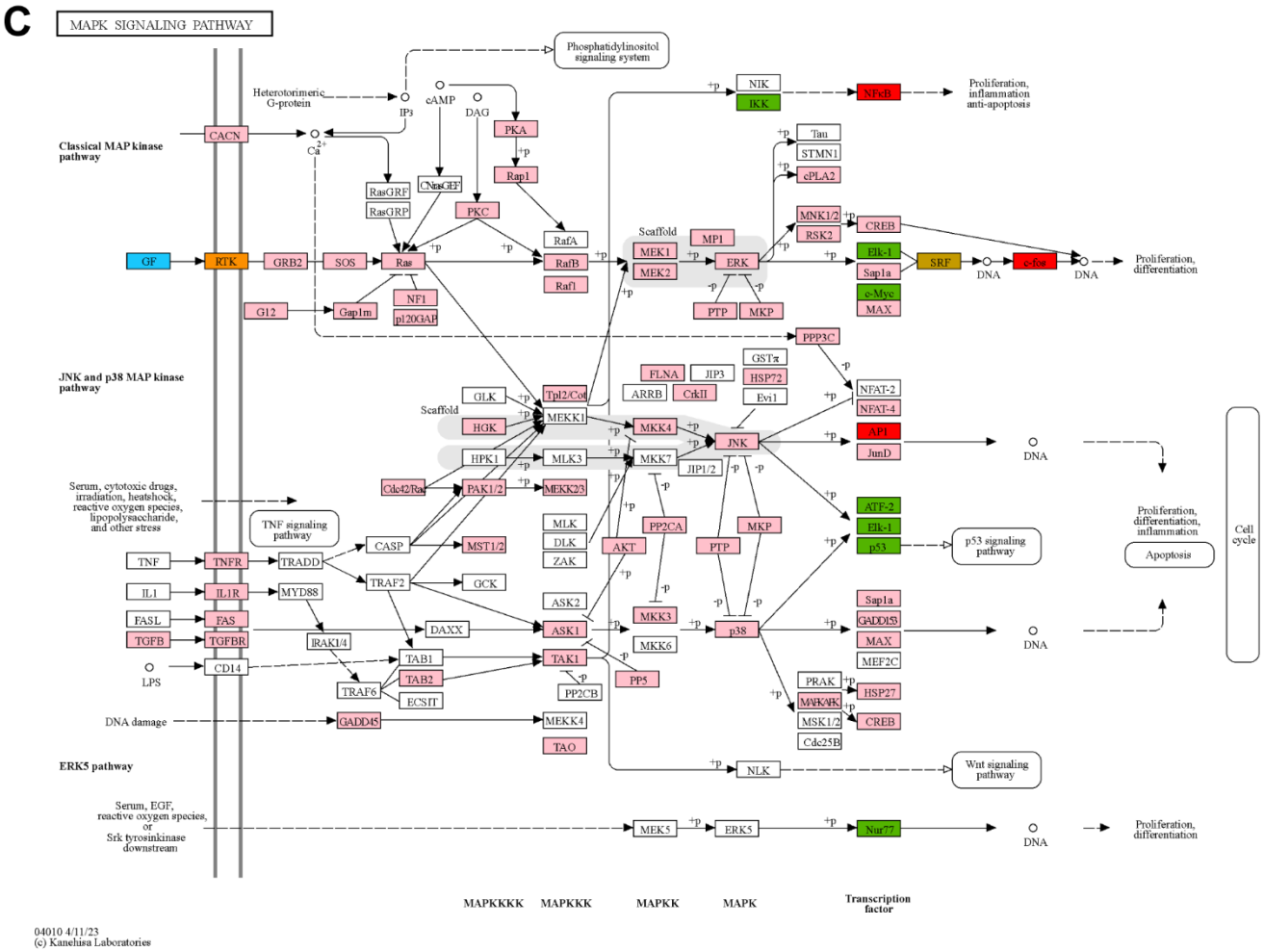

Figure 3—figure supplement 1. Involvement of GDNF signaling pathway in the nerve injury-sensing mechanism by cluster 1 FAPs.

(**A**) Top 10 genes specifically enriched in cluster 1 FAPs. *P* values were drawn from Wilcoxon rank sum test. (**B**) Results from g:Profiler showing pathways enriched using genes specifically enriched in cluster 1. (**C**) MAPK signaling pathway retrieved from KEGG, with color-coding to highlight relevant genes. Blue: GDNF ligand; orange: GDNF receptor RET expressed in cluster 1; pink: downstream cascade genes expressed in clusters 1-3; red: transcription factors (TFs) commonly predicted to regulate upregulated genes in clusters 2 and 3; green: TFs predicted to regulate genes upregulated in cluster 2; gold: TFs predicted to regulate genes upregulated in cluster 3.

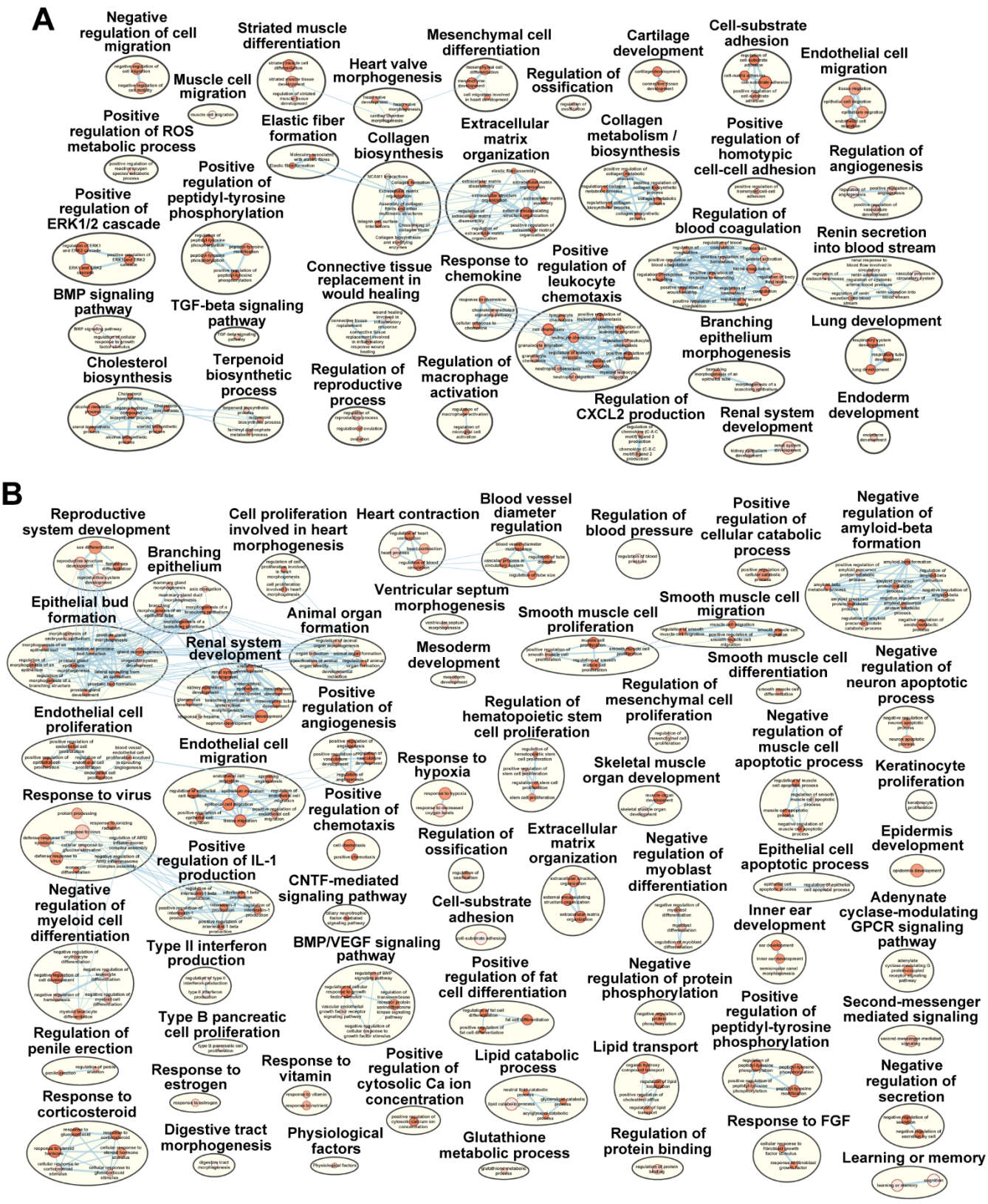

Figure 3—figure supplement 2. Pathways enriched in the two activated clusters within nerve injury-affected FAPs.

(**A**–**B**) Results from g:Profiler showing pathways enriched using genes specifically enriched in (A) cluster 2 or (B) cluster 3.

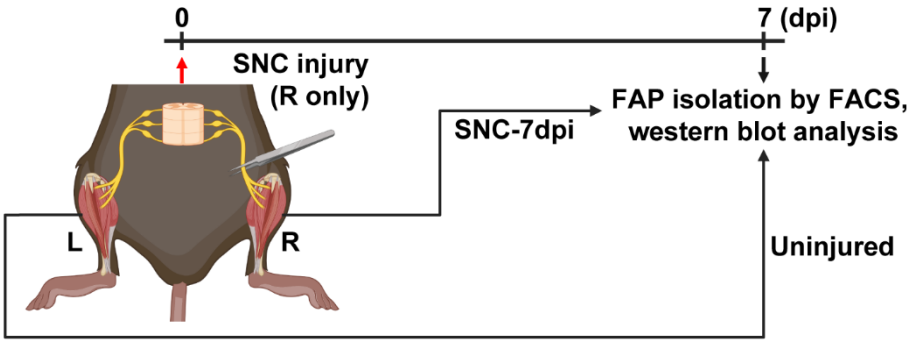

Figure 4—figure supplement 1. Scheme for western blot analysis.
Experimental scheme depicting sample collection for FAP isolation and the timeline for SNC and FAP isolation for the western blot analysis done in Figure 4F.

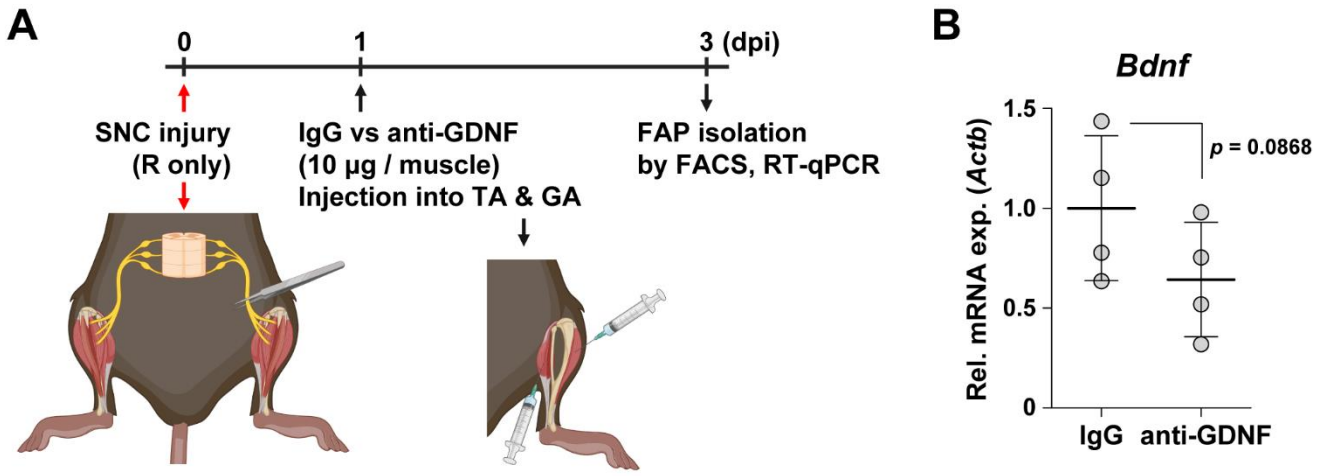

Figure 4—figure supplement 2. Decreased intramuscular GDNF activity can weaken *Bdnf* induction in FAPs upon nerve injury.

(**A**) Experimental scheme depicting intramuscular injection of either anti-GDNF antibodies or IgG control after SNC, along with the experimental timeline. (**B**) RT-qPCR results showing the expression levels of *Bdnf* in nerve injury-exposed FAPs affected by intramuscular injection of either IgG control or anti-GDNF antibodies. n = 4. Unpaired t-test.

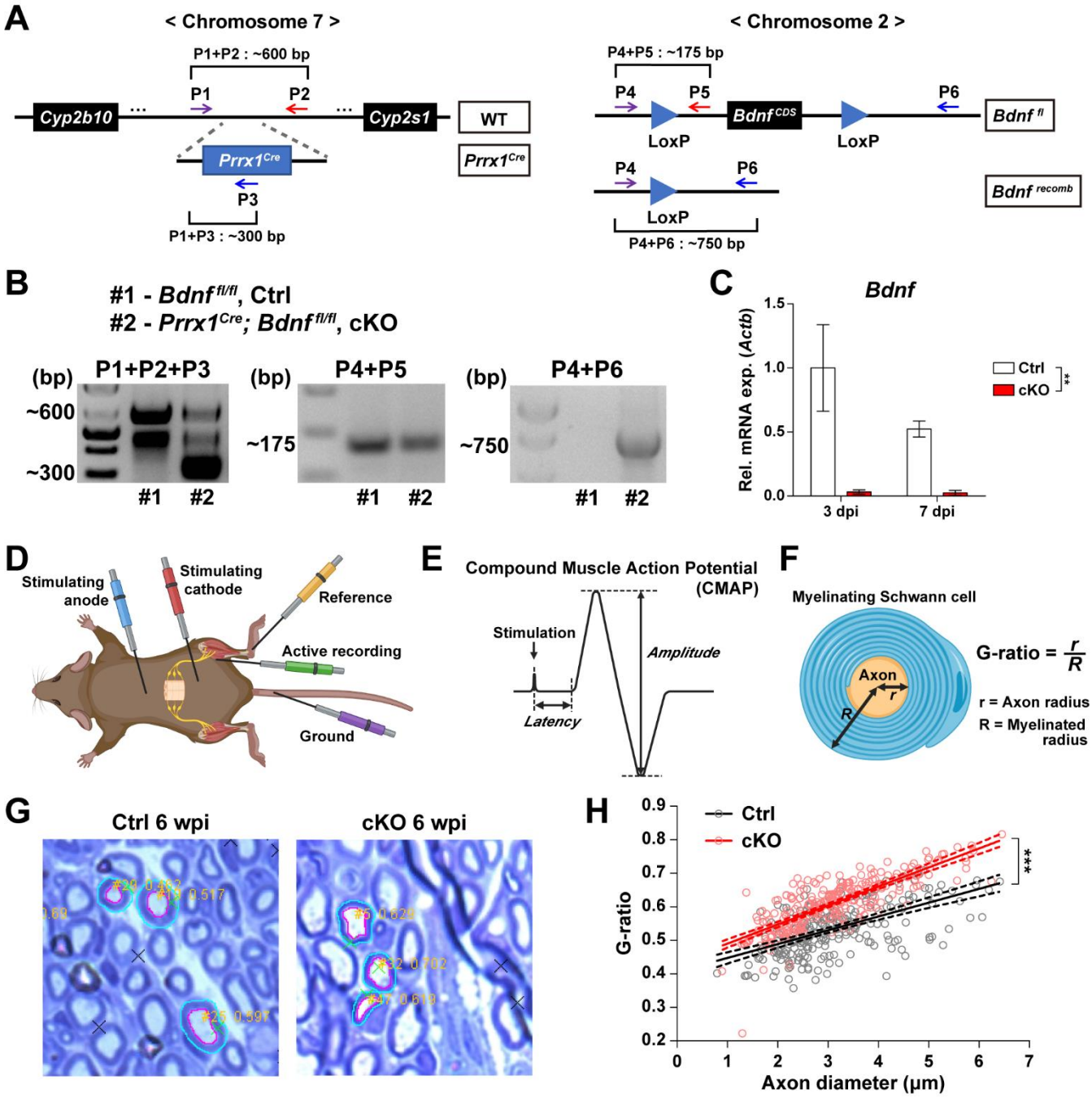

Figure 5—figure supplement 1. Validation of cKO mice used in this study and methods used for analysis. (**A**) Genomic loci and structure of *Prrx1*^{Cre} and *Bdnf*^{fl} alleles labeled with primers used for genotyping and genomic DNA recombination validation. (**B**) Results from genotyping (left and middle) and genomic DNA recombination PCR (right). Genomic DNA recombination of the LoxP flanking sites in the cKO mice were confirmed using primers P4 and P6 shown in (A). (**C**) RT-qPCR results of *Bdnf* expression using FAPs isolated from either Ctrl or cKO mice at 3 or 7 days post SNC. n = 2; Two-way ANOVA. ** $p < 0.01$. (**D**) Scheme for CMAP measurement showing the positions of electrodes used. (**E**) Diagram of a typical CMAP graph along with amplitude and latency used for analysis. (**F**) Diagram depicting calculation of G-ratio. (**G**) Examples of images from G-ratio quantification using ImageJ plugin GRatio for ImageJ. (**H**) Scatter plots with linear regressions displaying G-ratios (y-axis) in relation to axon diameters (x-axis). Solid lines are linear regressions and dotted lines represent error in 95% confidence level. ANCOVA, *** $p < 0.001$.

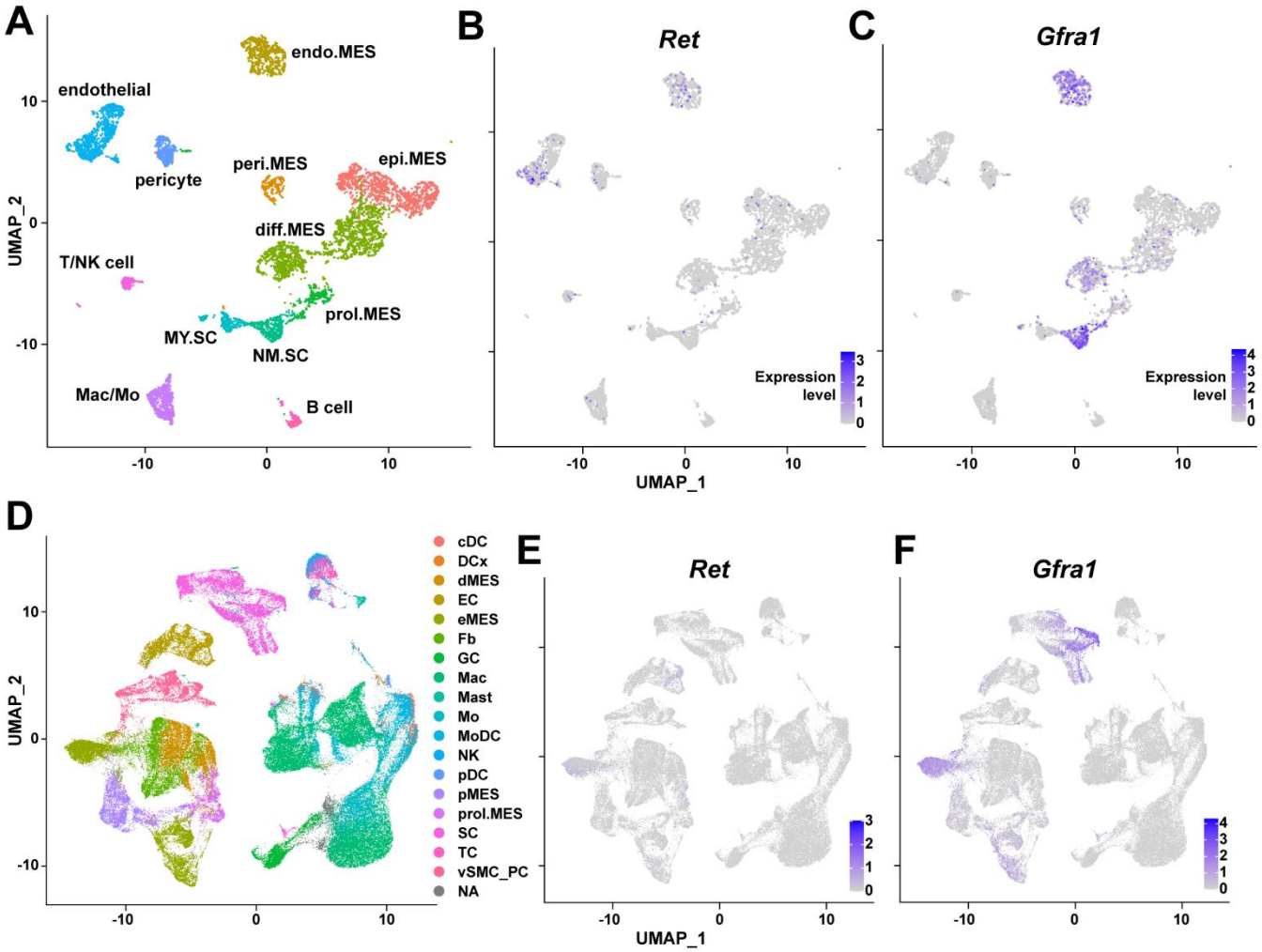

Supplemental figure 1. Expression of GDNF receptor genes *Ret* and *Gfra1* in nerve-resident cells. (**A**–**C**) scRNA-seq data from Carr et al. (2019) and Toma et al. (2020) (accession numbers: GSM3408137, GSM3408139, GSM4423509, and GSM4423506) were merged into a single Seurat object and visualized on UMAP plots. Cell types identified using markers listed by Toma et al. (2020) are shown in (A), and expression levels of (B) *Ret* and (C) *Gfra1* are displayed. epi.MES: epineurial mesenchymal cells; peri.MES: perineurial mesenchymal cells; endo.MES: endoneurial mesenchymal cells; diff.MES: differentiating mesenchymal cells; prol.MES: proliferating mesenchymal cells; NM.SC: non-myelinating Schwann cells; MY.SC: myelinating Schwann cells; Mac/Mo: macrophage/monocyte. (**D**–**F**) scRNA-seq data from Zhao et al. (2022) (accession number: GSE198582) were merged into a single Seurat object and visualized on UMAP plots. Cell types annotated by Zhao et al. (2022) are shown in (D), and expression levels of (E) *Ret* and (F) *Gfra1* are displayed. cDC: conventional dendritic cells; DCx: dendritic cells destined for homing; dMES: differentiating mesenchymal cells; EC: endothelial cells; eMES: endoneurial mesenchymal cells; Fb: fibroblasts; GC: granulocytes; Mac: macrophages; Mast: mast cells; Mo: monocytes; MoDC: monocyte-derived dendritic cells; NK: natural killer cells; pDC: plasmocytoid dendritic cells; pMES: perineurial mesenchymal cells; prol.MES: proliferating mesenchymal cells; SC: Schwann cells; TC: T cells; vSMC_PC: vascular smooth muscle cells/pericytes; NA: not applicable.

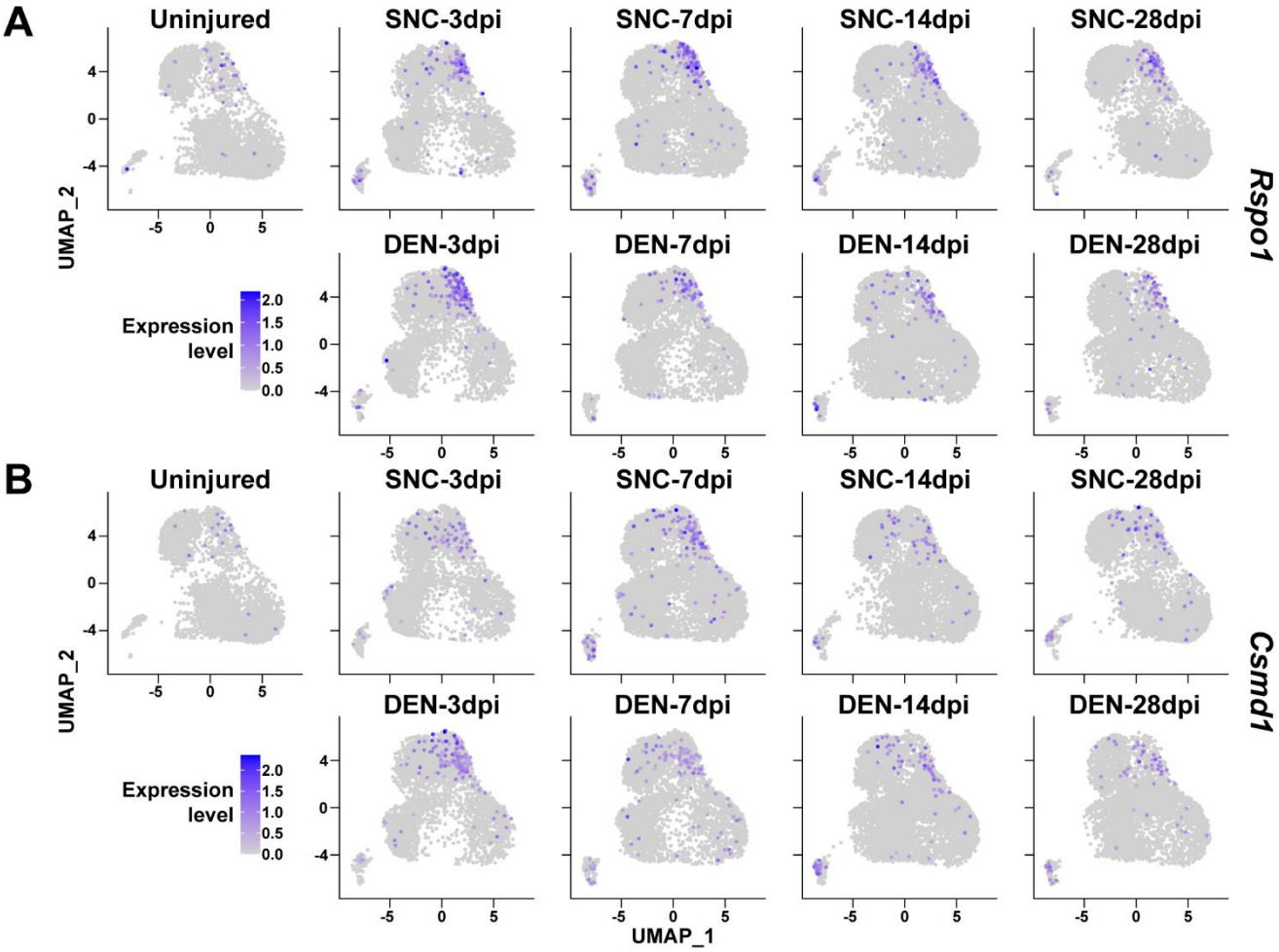

Supplemental figure 2. Expression of nerve injury-induced, cluster-specific genes in FAPs.
(**A**–**B**) Expressions of (A) *Rspo1* and (B) *Csmd1* shown on UMAP plots, separated by samples. scRNA-seq data obtained in this study were used.

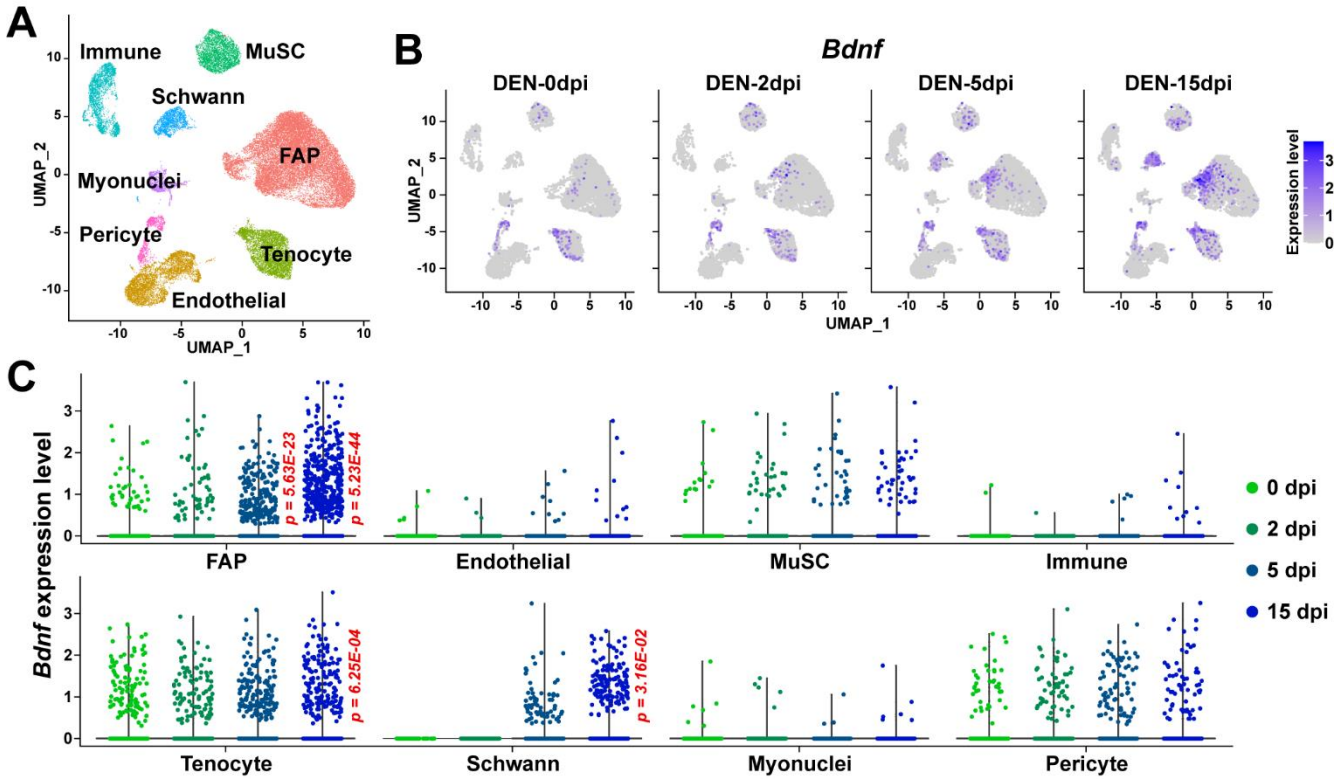

Supplemental figure 3. Expression of *Bdnf* in muscle-resident mononuclear cells affected by denervation. (**A**) UMAP plot showing data from Nicoletti et al. (2023) labeled by cell types identified. (**B**) Expression pattern of *Bdnf* in data from Nicoletti et al. (2023) shown on UMAP plots, separately by days post denervation. (**C**) Expression of *Bdnf* in each cell type on different days post denervation displayed in violin plots. *P* values were calculated by comparing each injury-affected cells' expression levels versus its uninjured state (0 dpi). Only significant *p* values are shown. Wilcoxon rank sum test.

Supplemental table 1. Results from TRRUST showing transcription factors predicted to regulate genes specifically enriched in cluster 2. Genes known to be regulated by each transcription factor is listed.

Key TF	Adjusted *P* value	List of overlapped genes
Jun	0.000114	Timp1, C1qtnf3, Plaur, Slc39a14, Mmp3, Itga5, Serpine1, Tgfb1, Mmp19, Ccl2, Slc8a1, Plau
Smad3	0.000399	Serpine1, Plau, Nedd9, Acta2, Ccl2, Tagln, Enpp1
Msx2	0.00464	Lss, Enpp1, Tagln, Alpl
Smad1	0.00579	Runx1, Col4a1, Col4a2, Tnfrsf11b
Ppard	0.00579	Angptl4, Tgfb1, Insig1
Sp1	0.00579	Acta2, Trf, Serpine1, Plaur, Lgals1, Mgp, Ccl2, Nes, Adcyap1r1, Itga5, Bmp4, Notch1, Skil
Fos	0.0149	Tgfb1, Bdnf, Tslp, Plau, Pdpn
Tgfb1i1	0.0149	Ccl2, Tgfb1
Srf	0.0185	Tagln, Barx2, Acta2
Id3	0.0298	Notch1, Alpl
Nfkb1	0.0298	Mmp3, Tgfb1, Dmp1, Pla2g4a, Il15, Egr2, Plaur, Ppp1r13l, Ccl2
Junb	0.034	Plau, Serpine1
Pparg	0.034	Serpine1, Muc1, Angptl4, C1qtnf3
Nfkb2	0.0362	Hif1a, Dmp1
Id1	0.0382	Thbs1, Alpl
Runx2	0.0382	Alpl, Mgp, Thbs1, Enpp1
Arntl	0.0382	Cxcl5, Bhlhe41
Msx1	0.0382	Tagln, Bmp4
Nr4a2	0.0382	Tnc, Gch1
Ets1	0.0388	Timp1, Mmp3, Ccl2, Bmp4
Prox1	0.0465	Pdpn, Notch1
Bcl3	0.0465	Runx1, Tnfrsf12a
Clock	0.0465	Serpine1, Bhlhe41
Etv4	0.0465	Mmp3, Plau

Supplemental table 2. Results from TRRUST showing transcription factors predicted to regulate genes specifically enriched in cluster 3. Genes known to be regulated by each transcription factor is listed.

Key TF	Adjusted *P* value	List of overlapped genes
Nfkb1	1.64E-05	Cxcl10, Tnfsf13b, Cebpa, Apoe, Cxcl1, Il12a, Myc, Vcam1, Tnf, Sox9, Plin2, Rel, Igf2bp2, Birc3, Hmox1, Nfkbiz, Bcl2
Cebpb	0.000206	Bcl2, Myc, Mafb, Cebpa, Btg2, Serpine1, Socs3
Sp1	0.000206	Ces1d, Myc, Mgarp, Serpine1, Sirt1, Cebpd, Egr1, Apoe, Cebpa, Slc2a3, Socs3, Adcyap1r1, Tnf, Ar, Lpl, Bmp4, Igfbp3
Dlx5	0.000206	Wnt5a, Alpl, Myc, Igfbp3
Stat3	0.000206	Mt1, Il12a, Pnp, Socs3, Bcl2, Cebpd, Egr1, Tnf, Myc
Rela	0.000206	Tnfsf13b, Myc, Vcam1, Igf2bp2, Birc3, Pgf, Sox9, Cxcl10, Apoe, Tnf, Bcl2
Stat1	0.000336	Cxcl9, Egr1, Mt1, Socs3, Cebpd, Cxcl10
Id1	0.000336	Thbs1, Alpl, Rel, Tnf
Crebbp	0.000876	Socs3, Fosb, Tnf, Hmox1, Bcl2, Mt1
Rel	0.00115	Cebpd, Birc3, Il12a, Tnf, Myc
Jun	0.00119	Plin2, Cebpd, Cxcl1, Serpine1, Hmox1, Aldh1a1, Tnf, Sirt1, Socs3, Plau
Hnf1b	0.00135	Mafb, Pde4c, Socs3
Hif1a	0.00324	Mt1, Cited2, Hmox1, Serpine1
Tfap2a	0.00381	Apoe, Cebpa, Meis1
Trp53	0.00595	Btg2, Thbs1, Hmox1, Bcl2, Mt1, Agtr1a, Myc, Serpine1, Egr1, Pappa
Ikbkb	0.00595	Cxcl9, Cxcl10, Tnf
Epas1	0.00678	Serpine1, Cited2, Vcam1
Ppara	0.00678	Cebpa, Lpl, Cebpd, Serpine1, Bcl2
Twist1	0.00781	Fgf10, Sox9, Tnf, Mme
Smad3	0.00809	Serpine1, Plau, Sirt1, Tnfsf13b, Myc
Bcl3	0.00899	Tnf, Cxcl10, Ubc
Atf2	0.0104	Sox9, Cebpa, Tnf
Fos	0.0127	Socs3, Tslp, Mt1, Plau, Egr1
Etv2	0.0146	Sox9, Plau
Mtf1	0.0146	Pgf, Mt1
Rbl1	0.0146	Myc, Alpl
Ctnnb1	0.0167	Bmp4, Isl1, Myc, Tbx3, Gja1
Elk1	0.0181	Hmox1, Egr1
Fosl1	0.0181	Thbs1, Thbs2
Dnmt3a	0.0209	Vtn, Mt1
Foxg1	0.0209	Ebf3, Serpine1
Id3	0.0209	Vcam1, Alpl
Tbx1	0.0209	Ripply3, Fgf10
Egr1	0.0225	Tnf, Serpine1, Thbs1, Nr4a1, Il12a
Irf1	0.0225	Cxcl10, Il12a, Tnf
Foxo3	0.0225	Socs3, Sirt1
Gfi1b	0.0225	Meis1, Socs3
Junb	0.0225	Plau, Serpine1
Ncoa3	0.0225	Igfbp3, Tbx3
Foxo1	0.0242	Bcl2l11, Egr1, Lpl, Alpl

(Continued)

Myc	0.0242	Myc, Cebpd, Bcl2, Zfp36
Pparg	0.0246	Serpine1, Plin2, Egr1, Hmox1
Nfkb2	0.0246	Myc, Rel
Nr4a1	0.0246	Serpine1, Ar
Nfe2l2	0.0278	Bcl2, Hmox1, Sult1e1, Mt1
Id2	0.0278	Alpl, Zbtb16
Klf5	0.0278	Egr1, Serpine1
Creb1	0.0312	Bcl2, Nfkbiz, Slc2a3
Runx2	0.0336	Alpl, Thbs1, Hbegf, Sox9
Ets1	0.0369	Egr1, Hmox1, Nr2f1, Bmp4
Ep300	0.0382	Tnfsf13b, Mt1, Hmox1, Socs3
Usf2	0.04	Hmox1, Mt1
Mecp2	0.0496	Slc2a3, Igfbp3
Stat6	0.0496	Tnf, Egr1

Supplemental table 3. Categorization of genes predicted to be regulated by transcription factors that act downstream of the GDNF signaling pathway. Note that only *Bdnf* fits into all three criteria.

Gene	Secreted	GO term related to neuron/glial cell regulation	Exclusive expression in activated FAPs
Bdnf	O	O	O
Apoe	O	O	X
Ccl2	O	O	X
Tgfb1	O	O	X
Tnf	O	O	X
Vcam1	O	O	X
Dmp1	O	X	O
C1qtnf3	O	X	X
Cxcl1	O	X	X
Cxcl10	O	X	X
Il12a	O	X	X
Il15	O	X	X
Mmp19	O	X	X
Mmp3	O	X	X
Plau	O	X	X
Plaur	O	X	X
Serpine1	O	X	X
Timp1	O	X	X
Tnfsf13b	O	X	X
Tslp	O	X	X
Bcl2	X	O	X
Egr1	X	O	X
Egr2	X	O	X
Hif1a	X	O	X
Hmox1	X	O	X
Igf2bp2	X	O	X
Mt1	X	O	X
Myc	X	O	X
Rel	X	O	X
Sirt1	X	O	X
Sox9	X	O	X
Aldh1a1	X	X	X
Birc3	X	X	X
Cebpa	X	X	X
Cebpd	X	X	X
Itga5	X	X	X
Nfkbiz	X	X	X
Pdpn	X	X	X
Pla2g4a	X	X	X
Plin2	X	X	X
Ppp1r13l	X	X	X
Slc39a14	X	X	X
Slc8a1	X	X	X
Socs3	X	X	X

Supplemental table 4. Primers used in this study for genotyping PCR or RT-qPCR.

No.	Primer	Usage	Sequence (5' to 3')
1	Prrx1Cre_com_R (P1)	Genotyping PCR	TAG TGA AGT GGA AGT TCC TGG
2	Prrx1Cre_WT_F (P2)	Genotyping PCR	CAG TTC CTA CCC TGA TTT CC
3	Prrx1Cre_Tg_F (P3)	Genotyping PCR	GAT CAT AAT CAG CCA TAC CAC
4	Bdnf_flox_F (P4)	Genotyping PCR	TGT GAT TGT GTT TCT GGT GAC
5	Bdnf_flox_R (P5)	Genotyping PCR	CGG TTT CTA AGC AAG TGA ACA
6	Bdnf_recomb_R (P6)	Genotyping PCR	GAA ATT TTC TCC ATC CCT ACT CCG GG
7	Cre_F	Genotyping PCR	GCA TTA CCG GTC GAT GCA ACG AGT GAT GAG
8	Cre_R	Genotyping PCR	GAG TGA ACG AAC CTG GTC GAA ATC AGT GCG
9	Rosa-tdT_WT_F	Genotyping PCR	AAG GGA GCT GCA GTG GAG TA
10	Rosa-tdT_WT_R	Genotyping PCR	CCG AAA ATC TGT GGG AAG TC
11	Rosa-tdT_Tg_F	Genotyping PCR	GGC ATT AAA GCA GCG TAT CC
12	Rosa-tdT_Tg_R	Genotyping PCR	CTG TTC CTG TAC GGC ATG G
13	Actb_qF	RT-qPCR	CCT CCC TGG AGA AGA GCT ATG
14	Actb_qR	RT-qPCR	TTA CGG ATG TCA ACG TCA CAC
15	Ret_qF	RT-qPCR	CCA GGG CTT CCC AAT CAG TT
16	Ret_qR	RT-qPCR	TTC CAA ACT CGC CTT CTC CC
17	Gfra1_qF	RT-qPCR	CAC TCC TGG ATT TGC TGA TGT
18	Gfra1_qR	RT-qPCR	AGT GTG CGG TAC TTG GTG C
19	Gdnf_qF	RT-qPCR	TCG GCC GAG ACA ATG TAT GA
20	Gdnf_qR	RT-qPCR	CAA CAT GCC TGG CCT ACT TTG
21	Bdnf_qF	RT-qPCR	AAG GAC GCG GAC TTG TAC AC
22	Bdnf_qR	RT-qPCR	CGC TAA TAC TGT CAC ACA CGC